ACS APPLIED MATERIALS & INTERFACES

Spotlight on Applications

www.acsami.org

Design of Functional Nanoparticles and Assemblies for Theranostic Applications

Zakiya Skeete,[†,‡] Hanwen Cheng,[†,‡] Elizabeth Crew,[‡] Liqin Lin,[‡] Wei Zhao,[‡] Pharrah Joseph,[‡] Shiyao Shan,[‡] Hannah Cronk,[‡] Jin Luo,[‡] Yongjun Li,[‡] Qunwei Zhang,[§] and Chuan-Jian Zhong*[,‡]

[‡]Department of Chemistry, State University of New York at Binghamton, Binghamton, New York 13902, United States

[§]Department of Environmental and Occupational Health Sciences, University of Louisville, Louisville, Kentucky 40292, United States

ABSTRACT: Nanostructured materials have found increasing applications in medical therapies and diagnostics (theranostics). The main challenge is the ability to impart the nanomaterials with structurally tailored functional properties which can effectively target biomolecules but also provide signatures for effective detection. The harnessing of functional nanoparticles and assemblies serves as a powerful strategy for the creation of the structurally tailored multifunctional properties. This article highlights some of the important design strategies in recent investigation of metals (especially gold and silver), and magnetically functionalized nanoparticles, and molecularly assembled or biomolecularly conjugated nanoparticles with tunable optical, spectroscopic, magnetic, and electrical properties for applications in several areas of potential theranostic interests. Examples include colorimetric detection of amino acids and small peptides, surface-enhanced Raman scattering detection of biomolecular recognition of proteins and DNAs, delivery in cell transfection and bacteria inactivation, and chemiresistive detection of breath biomarkers. A major emphasis is placed on understanding how the control of the nanostructures and the molecular and biomolecular interactions impact these biofunctional properties, which has important implications for bottom-up designs of theranostic materials.

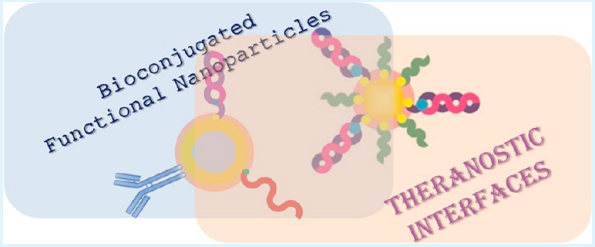

KEYWORDS: *gold nanoparticles, core–shell magnetic nanoparticles, assembly of nanoparticles, bioconjugation, SERS detection, flexible chemical sensors*

1. INTRODUCTION

Identification and intervention of biomolecules such as amino acids, proteins, DNAs, microRNAs, and bacteria are important for medical diagnostics. Among the various techniques for such diagnostics, the surge of interests in exploring gold or silver based nanoparticles as diagnostic probes stems largely from the unprecedented amplification of optical, spectroscopic, electrical and magnetic signals and their biofunctionality and biocompatibility. These capabilities are further enhanced by the controllable sizes, shapes, compositions and surface properties, especially conjugation with desired biospecificity or assembly with the desired signal transduction mechanism. Therefore, the exploration of gold-based nanoparticles (Au NPs) for detection, diagnostics, manipulation, targeting or transport of biomolecules is a topic of broad interest to drug delivery,[1,2] disease detection,[1] biosensing.[2,3] There are also increasing interests in exploiting nanoparticles' antimicrobial properties, including wound dressings, and biological responses.[4] One area of interest involves colorimetric detection of amino acids and small peptides, which are known to play different roles in heart disease, rheumatoid arthritis and AIDS.[5] For example, homocysteine is involved in the metabolism of methionine and is considered as a risk factor for heart disease.[5] Glutathione, a tripeptide, is known to protect red blood cells from oxidative damage, and plays an important role in the detoxification of the cell, as well as the removal of harmful organic peroxides and free radicals. L-Cysteine plays an important role in living systems and its deficiency is associated with a number of clinical situations (liver damage, skin lesions, AIDS, and certain neurodegenerative diseases). D-Cysteine, on the other hand, is believed to interfere with many targets inside the cell. A common characteristic of these biologically relevant amino acids, such as cysteine and homocysteine, and small peptides such as glutathione is the thiol group in the structure, which has a strong affinity to gold or silver surfaces. Their conjugation to gold nanoparticles and the unique interparticle interactions provide a means for colorimetric detection of these biologically relevant molecules.

The bioconjugation ability of gold nanoparticles, on the other hand, enables them to function as an intriguing drug carrier or vehicle, which is an important area of current interest. Upon entering biological systems, Au NPs function as a carrier to deliver biomolecules (e.g., miRNAs) in cell transfection, or as an antibacterial agent to inactivate bacteria, or potential toxic agent to damage biological functionalities (nanotoxicity). The importance of miRNA in the treatment of cancer and for the manipulation of genetic expression has been recognized. The

Special Issue: Materials for Theranostics

Received: May 5, 2014
Accepted: August 1, 2014
Published: August 11, 2014

   dx.doi.org/10.1021/am502693t | *ACS Appl. Mater. Interfaces* 2014, 6, 21752–21768

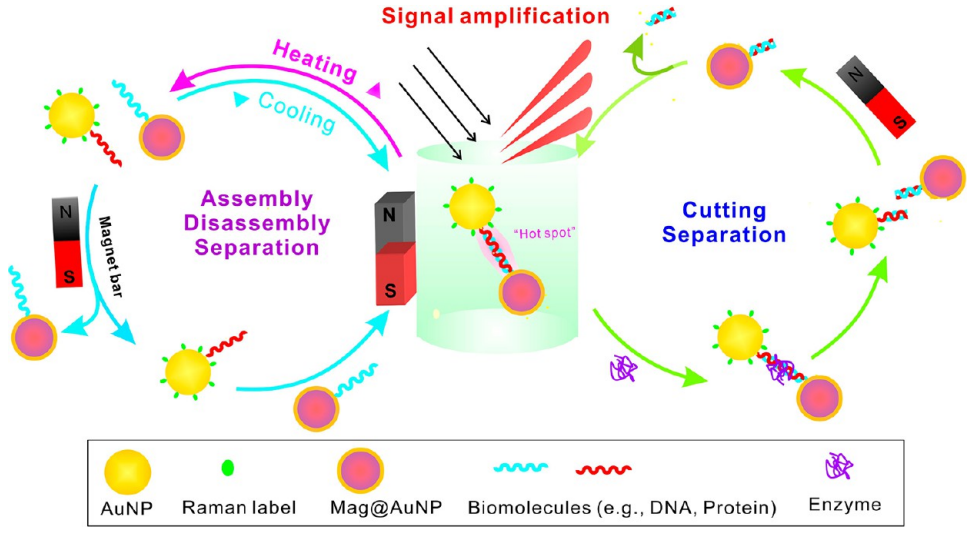

Figure 1. Illustration of bifunctional NPs for detection and magnetic intervention of biomolecular activities in a solution.

study of Au NPs as carriers of certain miRNAs (e.g., miR-130b), which express differently in glucocorticoid-sensitive versus glucocorticoid-resistant MM.1 cell lines, is one of the latest examples in cell transfection. Another area of current interest involves bacterial contamination of platelets, which is the leading cause of morbidity and mortality from a transfusion transmitted infection, and bacterial inactivation which is considered as an option to reduce infection risk.[6] There is an increasing need to understand the mechanistic details of the cell interactions of antimicrobial agents in microorganisms. Because of the high surface to volume ratio for a more efficient bacterial disinfection, nanoscale metal particles such as silver nanoparticles (Ag NPs) are widely studied in antimicrobial applications. The introduction of magnetic cores in silver nanoparticles enables effective separation and delivery of the antibacterial agents in biological systems.

In comparison with the exploration of metal nanoparticles as probes, carriers, or vehicles, one of the active research areas focuses on the assembly of nanoparticles. Broadly speaking, the assembly of nanoparticles is a result of the interparticle interactions leading to an association of the individual nanoparticles ranging from dimers or trimers to arrays or thin films. Such assemblies influence the collective optical or spectroscopic properties which can be harnessed for the detection of biomolecular recognition of proteins, DNAs, and other biomarker molecules. There have been increasing interests in nanoparticle-based approaches to DNA analysis largely because of the potential enabling spatial multiplexing in an array format to produce simple and portable biosensor devices. Among various techniques, surface enhanced Raman scattering (SERS) technique using Au and Ag NPs has emerged as one class of the highly sensitive spectroscopic probes for biomolecular detection.[7] It is the interparticle interaction or assembly that enables the creation of "hot spots" for the observation of SERS effect. Theoretical calculations have shown that the SERS effect is closely related to the local electric field enhancement around nanoparticles, especially near corners, edges or gaps (so-called "hot-spots"), that are responsible for its high sensitivity and fingerprinting capability.[8−11] Recent interests in exploring magnetic nanoparticle cores with gold or silver shells largely stem from the possibility of exploiting the unique combination of the SERS effect of Au or Ag NPs[8−10] and the nanoscale magnetic properties of magnetically active nanoparticles for biospecific separation, delivery, or targeting.

Indeed, the ability to impart magnetic functionality to gold or silver nanoparticles has led to increasing opportunities in the design of new strategies in theranostic applications. One important strategy for exploiting Au- or Ag-based nanoparticles involves an effective coupling of biomolecular detection and intervention (Figure 1).

For example, this strategy can be used for the recognition of complementary single-strand (*ss*) DNAs anchored to two different nanoparticles, i.e., Raman-labeled Au NPs and Au- or Ag-coated or -decorated magnetic NPs, and the enzymatic cutting of the double-strand (*ds*) DNA. The creation of "hot-spot" by the interparticle plasmonic coupling as a result of double-strand (*ds*) DNA linkage provides a means for SERS detection. This ability stems from interparticle distance-dependent local electric field enhancement (i.e., "hot-spot") in between NPs linked by *ds*-DNA (e.g., dimer), as demonstrated by theoretical modeling using discrete dipole approximation method.[10] Upon enzyme cutting of the *ds*-DNA at a specific site, the "hot spot" can be removed. On the other hand, the incorporation of a magnetic component in the nanoparticles provides the capabilities of easy intervention and bioseparation.

This type of functional nanoprobes could enable interparticle "hot spot" formation and bioseparation capabilities for monitoring DNA assembly and cutting processes in biological fluids in real time. The understanding of the effective coupling of the localized fields between particles and substrates[12] will be useful for diagnostics, drug delivery, and DNA separation,[13] including cetuximab conjugated magnetic core−shell nanoparticles for early detection of colon cancer, and bioassays of DNA cleavage and binding by human *p53* that may be useful for pathogen detection and disease analysis.[14] Although much has been learned about the DNA-conjugated nanoparticles for assays on solid substrates,[3,15,16] relatively little is known about monitoring the detailed processes related to protein binding and cutting of DNAs in a biologically relevant solution phase.[14,17] The assembly of Au NPs by complementary-strand binding of DNA designed using the *cyclin G* promoter sequence for *p53* recognition leads to the formation of a double strand in between Au NPs, which provides a *p53* recognition site. It also provides a recognition site for a restriction enzyme that cuts the *ds*-DNA at a

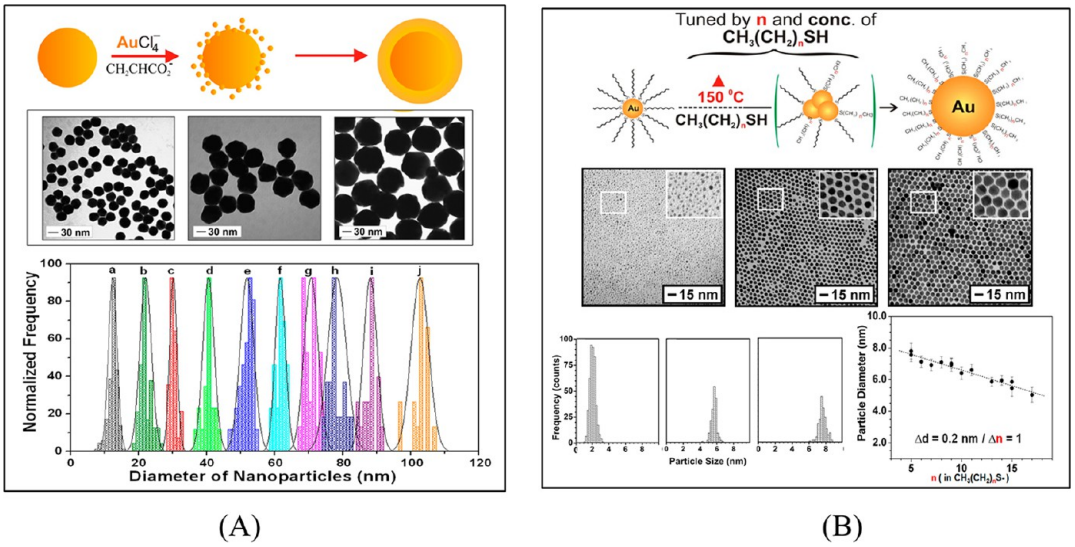

Figure 2. (A) Seeded and aggregative growth of Au NPs (top scheme) as shown by the growth from 30 nm seeds to 60 and 90 nm Au NPs (from left to right in the TEM images), and size distributions (bottom panel). (B) Thermally activated aggregative growth of Au NPs capped by alkanethiolate monolayer, TEM of Au NPs produced by thermal processing of DT-capped Au NPs (left, 2.01 ± 0.41 nm) in the presence of alkanethiols of different chain length (*n*, from middle to right): *n* = 5 (7.60 ± 0.43 nm) and *n* = 15 (5.86 ± 0.31 nm), size distributions (bottom left), and dependence of particle size on capping alkyl chain length (bottom right). Reproduced with permission from refs 12 and 37. Copyright 2006 and 2010 American Chemical Society.

specific site, allowing the use of nanoparticle assembly as a probe to the interactions and relativities of the *ds*-DNA directly in a solution.[14]

The signal amplification and fingerprinting capability of SERS have led to increasing interests in studies of nanomaterials of different sizes, shapes and structures, especially gold or silver NPs for various applications.[18] The exceptionally strong confinement of electromagnetic energy around plasmonic-active metal nanoparticles exhibits approximately fourth power of the field enhancement at the particle surface, especially in the vicinity of sharp features or small gaps in nanostructures. The synthesis of pure dimers is a challenge, but there have been several intriguing approaches to controlling the enhancement gap (e.g., gold nanogap particles[18]). Indeed, various nanostructures of Au and Ag have been extensively exploited for SERS, which has rapidly emerged as highly sensitive colorimetric and spectroscopic techniques for the detection of DNAs, proteins or enzymes.[6,8,12,14,19−22] In comparison with solid-state SERS substrates for antibody−antigen binding of Au NPs on a gold thin film,[20,21] the enhancement of SERS using nanoparticles suspended in a solution[12,20] is smaller, but understanding the interparticle plasmonic coupling ("hot-spot") as a result of the formation of small clusters of nanoparticles such as dimers and trimers[20] is useful for developing the capability for biomolecular signal transduction and activity intervention in a solution phase. Considering the limited surface modification and potential nanotoxicity of magnetic nanoparticles (MNPs, e.g., iron, nickel, or cobalt oxides) in bioseparation and controlled delivery,[23] or magnetic resonance imaging (MRI),[24] there is an increased interest in introducing desired surface functionalization of MNPs using gold or silver as a shell. This type of surface chemistry has been demonstrated for biomolecular separation from solutions,[12,20−22] cancer-cell targeting,[25] and SERS detection.[26] The detection in these studies involved using solid substrates or magnetic enrichment. Recent insights into the reactivity of restriction enzyme at DNA-mediated assembly of Au NPs in a solution phase have demonstrated the possibility of the nanoprobes strategy for potential *p53* protein recognition.[24]

Another pathway for exploring the assembly of nanoparticles as functional materials involves molecularly mediated thin film assemblies of metal nanoparticles as sensing materials for electrical detection of volatile organic compounds (VOCs), which has potential application in the detection of breath biomarkers linked to different diseases, including diabetes[27] and lung cancers.[28] In addition to 4−5% more CO_2 and 4−5% less O_2 inhaled, vapors and trace gases include 5% H_2O, a few ppm (V) of H_2 and CO_2, NH_3 and acetone, methanol, ethanol, and other VOCs.[29] The detection of biomarkers from breath samples of patients with different diseases has attracted increasing interests. One example involves detection of acetone as a breath biomarker from diabetes, which has been identified to link to the level of blood sugar. Traditionally, GC and GC−mass spectroscopy have been used in breath sample analysis for diabetes, cancer, and oxidative stress in diabetes. In contrast to existing serum or urine analysis, the breath analysis features noninvasiveness and real-time monitoring. The development of nanoparticle-structured sensor arrays for breath analysis could lead to a potential point-of-care diagnostic tool.

Overall, there have been major advances in many areas exploring nanoparticles and assemblies for potential diagnostic applications, including latest examples in infectious disease detection, cancer diagnostics and imaging, and cancer biomarker detection,[30] which exploit optical and spectroscopic signals because of DNA and protein adsorption and assembly[31] and interparticle spacing or aggregation. Several recent reviews have discussed different nanostructure bioconjugation and plasmonic nanoparticle based biosensing[32,33] and therapeutic applications. Rather than comprehensively describing the exploration of nanoparticles for various applications in theranostics, which have been discussed in a number of recent reviews, each focusing on a different aspect, this article focuses on harnessing functional nanoparticles and assemblies as a strategy for the creation of the structurally tailored multifunctional properties for biomolecular

detection and intervention. In addition to describing progress in synthesis and processing of metal and magnetically functional nanoparticles and assemblies, examples in colorimetric detection of amino acids and small peptides, SERS detection of biomolecular recognition of proteins and DNAs, targeted delivery in cell transfection and bacteria inactivation, and nanostructured flexible sensor array for the detection of biomarkers of human breath will be highlighted.

2. SYNTHESIS, BIOCONJUGATION, AND ASSEMBLY OF NANOPARTICLES

2.1. Gold or Silver-Based Nanoparticles. The synthesis of Au NPs generally involves wet-chemical reduction of chloroauric anions ($AuCl_4^-$) as the gold precursor. For the synthesis of Au NPs in aqueous phase, seeded growth method have been reported for controlling particle size, most of the methods have been based on the modification of Turkevich method through a two-step process (two-step process: (1) nucleation and (2) growth). For the control of size, which is often difficult, a highly effective method was developed in our laboratory for the growth of highly monodispersed Au NPs in the size range of 10−100 nm diameter,[12] which involves $AuCl_4^-$ as a starting Au-precursor and acrylates as both reducing and capping agents in a seeded "aggregative growth" process. This is in contrast to Ostwald ripening, where smaller particles dissolve preferentially with subsequent crystallization onto larger particles. Insights into the growth mechanism were gained by the determination of the size and optical properties as a function of the growth parameters such as the reaction time and the seed/precursor concentrations,[11] demonstrating the operation of the aggregation growth mechanism in this simple and reproducible growth process. Au NPs with average sizes in 10−100 nm range can be easily grown using smaller particles as seeds (Figure 2A). The overall morphology of these nanoparticles is consistent with the polycrystalline characteristic. The size monodispersity is evident by narrow size distributions (Figure 2A). The relative standard deviations (RSD) are ∼8% for the smaller-sized (<30 nm), ∼4% for the medium-sized (30−50 nm), and ∼3% for the larger-sized (>50 nm) nanoparticles. The mass of the seed-grown particles is quantitatively correlated with the concentration of $AuCl_4^-$. By analysis of the correlation of nucleation parameters with the particle sizes and distributions, the growth was shown to follow a "seeded and aggregative growth" mechanism, which is consistent with the general characteristics of aggregative growth mechanism.[34]

For the synthesis of Au NPs in organic phase,[35] a key process in the Brust−Schiffrin Method for thiol-protected Au NPs, reported first in 1994, is to transfer $AuCl_4^-$ from aqueous phase to toluene using tetraoctylammonium bromide (TOABr), where it is reduced by sodium borohydride ($NaBH_4$) in the presence of dodecanethiol.[36] The resulting particles are in the range of 2−5 nm. A further modification of this method by manipulating the reaction temperature to control the size down to about 1 nm or introducing different capping ligand structures. The smaller-size characteristic is perhaps one of the main attributes in comparison with Au NPs synthesized in aqueous phases. Starting from nanoparticles synthesized by this route, one of the approaches to size control developed in our laboratory exploits the nanoscale phenomenon of melting point decrease for certain metal nanoparticles,[37,38] which is inversely proportional to the particle size and free energy reduction driven coalescence of surface-melting particles, leading to the increase of particle size. For example, alkanethiolate-capped Au NPs can be obtained by thermal activation of smaller-sized starting particles, e.g., decanethiolate (DT) capped Au NPs ($Au_{2\ nm}$-DT, 1.9 ± 0.7 nm), via shell desorption, core coalescence, and shell re-encapsulation in a toluene solution containing TOABr and capping molecules such as DT under controlled temperature (149 ± 1.5 °C) toward larger-sized nanoparticles.[38] The size distribution is strikingly narrow (Figure 2B). The uniform interparticle spacing between the nanoparticles with a predominant hexagonal packing array feature shows an edge-to-edge distance of ∼1.0 nm, corresponding closely to the distance expected for an interdigitation of alkyl chains between shells of the neighboring nanoparticles (Figure 2B).[38]

The thermally activated processing of a solution of presynthesized nanoparticles involves coupling of the molecular capping and re-encapsulation to the interparticle coalescence, different from simple Ostwald ripening processes. The particle size growth is shown to be a function of chain length of the capping alkanethiols ($CH_3(CH_2)_nSH$) (Figure 2B).[33,37] The cores of nanoparticles evolved using shorter chain thiols were found to be larger than those evolved in the presence of longer thiols. For example, using alkanethiols with n = 15 (Figure 2B), an average core diameter of 5.86 ± 0.31 nm was obtained. Since our early demonstration of this strategy for producing highly monodispersed Au NPs,[38] it also showed viability for processing copper and other metal nanoparticles. Using this approach with slight modifications, gold-based alloy and other metal (e.g., copper) nanoparticles of different sizes have also been prepared.[38] The molecularly tuned size selectivity[37] provides an important means for processing nanoparticle size and monodispersity.[38] In addition, depending on the alkanethiol concentration, the size of the nanoparticles after the thermal treatment is linearly dependent on the chain length of alkanethiols used (Figure 2B), exhibiting a slope of −0.2 nm/methylene unit. This correlation demonstrates the important role played by cohesive interactions in regulating interfacial reactivities of nanoparticles for the control of particle sizes, in contrast to a chemical synthesis route from precursor molecules.[36,39] In fact, deep insights into the importance of aggregative growth mechanism for the control of Au NPs size have recently been gained in both experimental and theoretical studies of the kinetics and mechanism for the size evolution of Au NPs under the thermally activated evolution process.[34,40] By using the well-known KJMA model for aggregative growth, a straightforward analytical method was derived for analysis of the growth kinetics. The method allows extraction of separate aggregative-nucleation, aggregative-growth, and Ostwald-ripening rate constants. The established aggregative nucleation rate and size distribution are contrasted to classical LaMer nucleation and growth, in addition to Ostwald ripening. In aggregative growth, which is a nonclassical nucleation and growth process, the nucleation parameters can be systematically varied by conditions that influence the stability of the initial small particles, leading to controlled size and distribution.

Similar approaches have also been used for the synthesis and processing of silver and gold−silver alloy nanoparticles.[41] In the synthesis of silver and gold−silver alloy nanoparticles encapsulated with alkanethiolate monolayer,[41] two-phase reduction of $AuCl_4^-$ (in toluene) and $AgBr_2^-$ (in toluene) is used.[42] The synthesis can be carried out by separately transferring $AgBr_2^-$ and $AuCl_4^-$ from aqueous phase to organic phase using TOABr as the phase transfer reagent. Different compositions of alloy nanoparticles were synthesized by controlling the feed ratios of the two metal precursors. The size monodispersity is better than

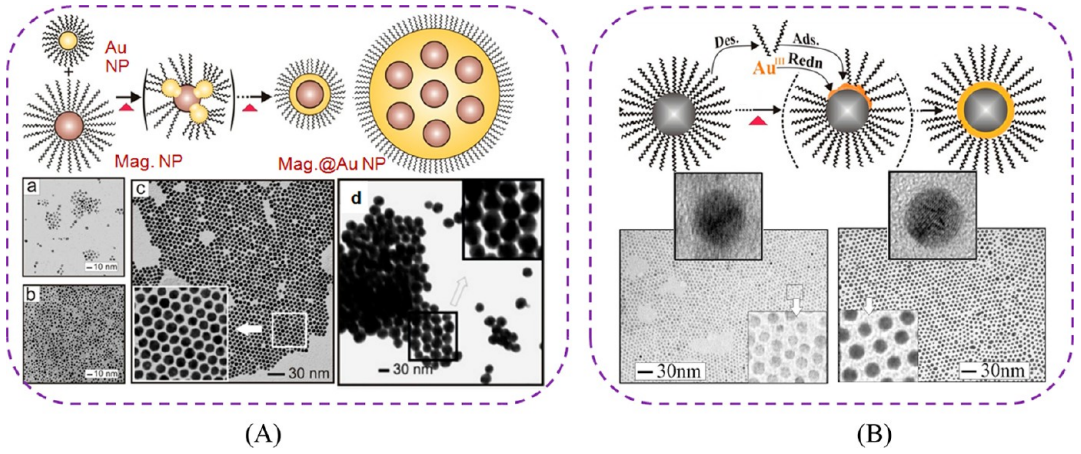

Figure 3. (A) Thermally activated aggregative growth (top scheme) showing the evolution from a mixture of (a) Au and (b) Fe_2O_3 precursor nanoparticles to (c, d) Fe_2O_3@Au NPs of different sizes. (B) Preparation route by combining bottom-up synthesis and thermal processing in a seeded-growth process (top scheme) involving the desorption (Des.) and adsorption (Ads.) of capping molecules and reduction of Au(III) and its deposition on Fe_3O_4 seeds (bottom left, 5.2 ± 0.4 nm) forming Fe_3O_4@Au NPs (bottom right, 6.6 ± 0.4 nm). Reproduced with permission from refs 21 and 43. Copyright 2005 and 2007 American Chemical Society.

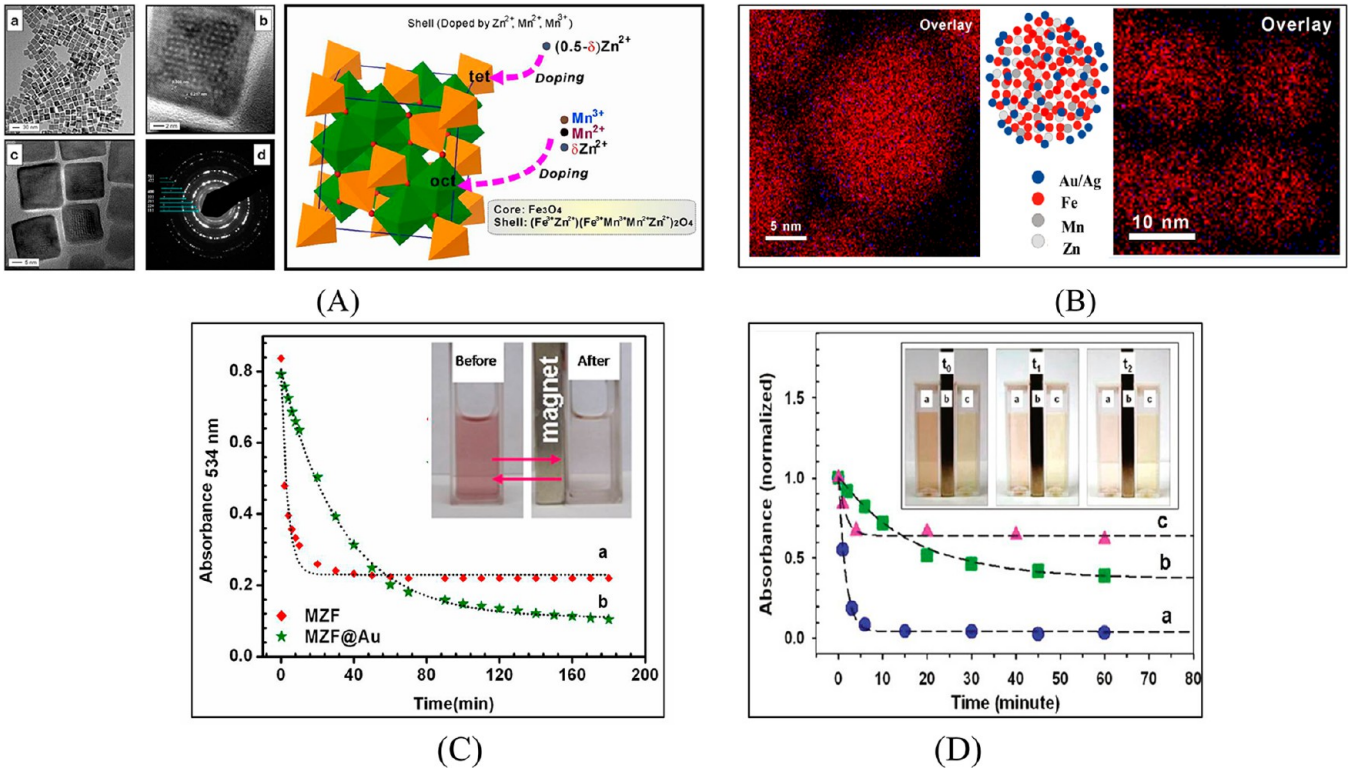

Figure 4. (A) Morphologies of MnZn ferrite (MZF) core−shell nanocubes: (a−c) TEM/HRTEM and (d) ED pattern for MnZn ferrite nanoparticles (size: 20.6 ± 1.8 nm, core (Fe_3O_4)/shell (($Mn_{0.5}Zn_{0.5}$)($Fe_{0.9}Mn_{1.1}$)O_4)). Right: structural model for MZF nanocubes consisting of Fe_3O_4 core (inverse core) and MZF shell where the tetrahedral sites are doped by (0.5-δ) Zn^{2+}, whereas the octahedral sites are doped by Mn^{3+}, Mn^{2+}, and the rest Zn^{2+}.[47] (B) EDS composition mapping for MZF@Au (left) and MZF@Ag (right) nanoparticles in terms of overlapping of Fe (red) with Au (MZF@Au) and Ag (MZF@Ag). Mn and Zn detected are not shown.[17] (C, D) Plots showing the magnetic separation kinetics in terms of the change in absorbance of SP band at (C) ~534 nm for a solution of (a) MZF and (b) MZF@Au (C),[17] and (D) ~420 nm for solutions of (a) MZF, (b) MZF@Ag, and (c) mixed MZF and Ag NP.[6] (Insets: photos showing color changes of solutions (a) and (c) before and after applying a magnet (b), leading to gradual separation (t_0 = 0; t_1 = 30; t_2 = 60 min).) Reproduced with permission from refs 6 and 47, Copyright 2010 and 2011 American Chemical Society, and from ref 17, Copyright 2013 Royal Society of Chemistry.

those synthesized by citrate reduction of Ag^+ in aqueous solutions. The alkanethiolate-capped Ag and AgAu NPs also allow the thermally active processing to achieve the controllability of particle size in the range of 2−10 nm.

2.2. Magnetically Functionalized Nanoparticles. In combination with various synthesis methods, the thermal activation strategy has also been demonstrated for controlled processing of metal, alloy, and core−shell nanoparticles in solutions in terms of size and morphology under an elevation of

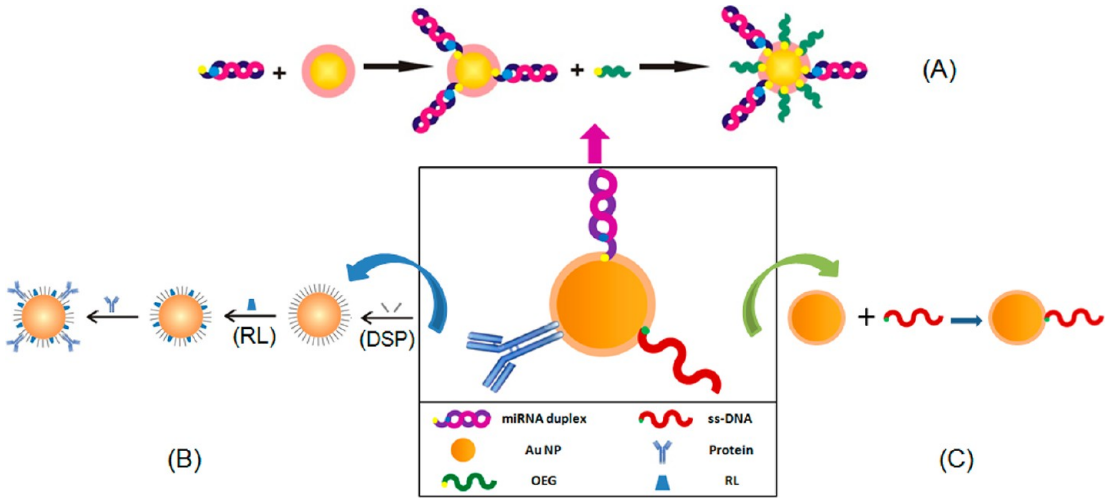

Figure 5. Illustrations of bioconjugation on Au NPs with (A) thiol-containing miRNA duplexes consisting of sense and antisense miRNAs (labeled with a fluorescent dye (e.g., Cy5)) along with oligoethylene glycol thiol (OEG) to keep the miRNAs from folding and electrostatically binding, (B) proteins (e.g., antibody) via a linking molecule (e.g., DSP (dithiobis (succinimidyl propionate))) along with a Raman label (RL) as a reporter, and (C) thiol-functionalized DNA.

temperatures ranging from 100 to 200 °C. Examples include Au, Cu, AuAg, AuCu, AuPt, and Fe_2O_3 or Fe_3O_4@Au.[37,38] By a combination of the lowered melting temperature for metal nanoparticles and the unaffected melting temperature of iron oxide nanoparticles, a thermally activated heterointerparticle coalescence was demonstrated for fabricating core@shell type of Fe-oxide@Au) nanoparticles.[21,43] One example involves the formation of Fe_2O_3 or Fe_3O_4 and Au nanoparticles in a solution by thermally activated heterointerparticle coalescence between gold and Fe_2O_3 or Fe_3O_4 nanoparticles under encapsulating environment (Figure 3A). The stabilization of the nanoparticles is achieved by organic ionic materials such as tetraoctylammonium bromide (TOABr) in the solution and the capping molecules such as alkanethiols (e.g., decanethiols (DT)) for Au nanoparticles and oleylamine and/or oleic acid for Fe-oxide nanoparticles. The thermal microenvironment facilitates core−shell coalescence to produce monodispersed Fe-oxide@Au nanoparticles of controlled sizes, depending on the relative ratio of the two precursors. It is the combination of the solution temperature, the composition, and the capping structures, along with the competition between growing Au and Fe-oxide@Au NPs, that leads to the formation of larger-sized core@shell nanoparticles with a single or multiple Fe-oxide cores (pomegranate-like) (Figure 3A).

The magnetic core−gold shell nanoparticles can also be prepared by combining wet-chemical synthesis and thermal processing in a seeded-growth process.[21,43,44] Figure 3B shows an example for the synthesis of monodispersed Fe_2O_3@Au and Fe_3O_4@Au nanoparticles,[43,45] using Fe_3O_4 seeds capped with oleylamine and/or oleic acid chemical reduction of Au-$(CH_3COO)_3$ in the presence of capping agents at 180 °C. The formation of core−shell nanoparticles is supported by the change in particle sizes in TEM and HR-TEM images (Figure 3B), the observation of Au-shell specific surface chemistry, the change in magnetization and blocking temperature, and the demonstration of their use in magnetic bioseparation or as spectroscopic probes.[21,44] The latter also involved many other core−shell types of magnetic or metal nanoparticles (e.g., MnZnFeO@Au, Fe_3O_4@Au@Pt, Pt@Au, AuAg, AuPt, PtVFe, PtNiFe[20,41,44−46]).

To achieve tunable nanomagnetism, MnZn ferrite nanomaterials with a spinel structure represent an important class of tunable magnetic materials.[47] In comparison with binary MFe_2O_4 (M = Fe, Co, Mn, Zn, etc.) nanoparticles,[48] MnZn ferrite nanoparticles provide an increased tunability. A novel core−shell structured nanocube of MnZn ferrite was synthesized by controlling reaction temperature and composition in the absence of conventional reducing agents in one-pot synthesis. The highly monodispersed and cube-shaped core−shell structure consists of an Fe_3O_4 core and an $(Mn_{0.5}Zn_{0.5})$-$(Fe_{0.9}Mn_{1.1})O_4$ shell (Figure 4A). The HR-TEM for the core−shell structure shows a Moiré pattern, indicating a highly crystalline combination of core and shell with slightly different lattice constants or rotation of the core relative to the shell.[47] In Figure 4B, two different phases are revealed, corresponding to a core of Fe_3O_4 and a shell of MnZn ferrite $(Mn_{0.5}Zn_{0.5})$-$(Fe_{0.9}Mn_{1.1})O_4$. They can be either antiferromagnetic or ferrimagnetic because of the antiparallel arrangement of the ions on the tetrahedral vs. the octahedral sites, resulting in the saturation magnetization of ∼96.5 emu/g. The highest value of magnetization, 45.6 emu/g, is close to the maximum magnetization value for Fe_3O_4 (5.2 nm) (66 emu/g).[43] The MnZn ferrite nanoparticles could also be synthesized in aqueous solutions, but the controllability over size monodispersity and shape is rather limited.[44]

The MnZn ferrite nanoparticles have been coated with Au or Ag shells of various thicknesses by seeded growth method.[21,44] In this method,[20] 35 nm MnZn ferrite core size was coated with 1.2 nm Au shell.[21] In a recent study,[17] the thermally activated processing method was used[21] for the preparation of Au- and Ag-decorated MZF nanoparticles, by heating a concentrated toluene solution with Au-DT (or Ag-DT) and OAM/OA-capped MZF nanoparticles in a certain ratio at 150 °C. The distributions of Fe, Mn, Zn, and Au or Ag are shown by the EDS data for MZF/Au and MZF/Ag NPs. There is clear indication that Au or Ag metals are decorated on the MZF core, as evidenced by overlapping Fe and Au in the case of MZF/Au or Fe (Figure 4B) and Ag in the case of MZF/Ag. The functional properties of these magnetic core−shell type NPs are also observed by a gradual decrease of the surface plasmon resonance bands of the NPs under a

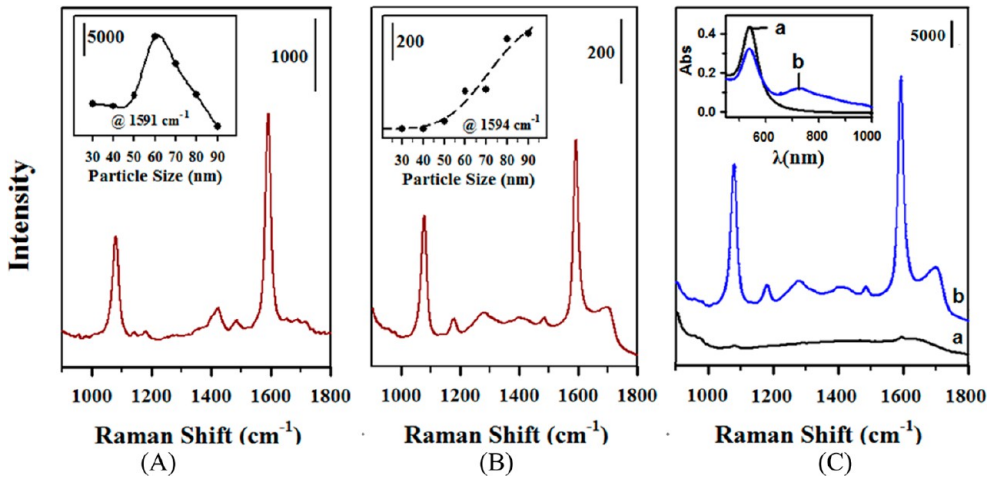

Figure 6. SERS spectra for (A) MBA-labeled $Au_{90\ nm}$ on a Au-film substrate (inset, SERS intensity at 1591 cm^{-1} vs particle size); (B) MBA-labeled $Au_{90\ nm}$ in aqueous solution (inset, SERS intensity at 1594 cm^{-1} vs nanoparticle size); and (C) solutions of MBA in the presence of $Au_{60\ nm}$ after centrifuging at different speeds: (a) 2000 and (b) 14 000 rpm (inset, UV−vis spectra for the corresponding solutions). Reproduced with permission from ref 20. Copyright 2008 IOP science.

magnetic field (Figure 4C), similar to those reported recently.[6,21] For example, a gradual decrease in the SP band absorbance is observed in Figure 4D for MZF@Ag nanoparticles, revealing clear differences for MZF@Ag, mixed MZF and Ag, and MZF. The magnetic properties are also evidenced by the decrease in color for MZF@Ag NPs in the solutions under the magnetic field.

2.3. Bioconjugation of Nanoparticles. The rich surface chemistry is one of the key attributes of Au- or Ag-based NPs that enables bioconjugation of thiol-containing amino acids, small peptides, proteins, miRNAs, and DNAs in effective ways (Figure 5). Gold nanoparticles can be conjugated with microRNA (miRNA) for delivery into cells for genetic manipulation or cellular marking.[49,50] Figure 5A shows an example in which Au NPs are conjugated with Cy5 (or Cy3) labeled miR-130b on the Au NPs (miRNA-AuNPs).[51] The dye molecules could serve as fluorescent or SERS labels.[9,12,20] Upon conjugation, the miRNA-AuNPs show an increased mobility in gel electrophoresis, consistent with the increased negative charge on the nanoparticle surface by miRNA. By performing ligand exchange reaction of miRNA-AuNPs with bis(*p*-sulfonatophenyl)phenylphosphine (BP), a negatively charged surfactant used for increasing the surface charge,[20] in the solution, the mobility remains unchanged, indicating that the miRNA-conjugation is quite stable.

Effective conjugation of protein molecules (antibody or antigen) and Raman label to nanoparticle surfaces is important for SERS-based immunoassay. As shown in Figure 5B, Au NPs can be labeled with Raman label and protein by controlled concentrations of dithiobis(succinimidyl propionate) (DSP), mercaptobenzoic acid (MBA), and protein A. This approach is relatively simple for controlling the coverage of MBA on the surface, and also has some flexibility in terms of the sequence of immobilizing MBA and protein.[21] Similar to homocysteine-mediated assembly of Au NPs,[52] the control of salt concentration in the solution is also important in determining the stability of the nanoparticles in an aqueous system, which is dependent on the chemical nature of capping molecules and the electrical double layer charges.

DNA-based nanoparticle assembly[13,53,54] is another important area exploiting the optical properties of the nanoparticles for the detection of enzymes and proteins associated with diseases and pathogens. For example, *p53* protein, a DNA binding protein, is found in more than 50% of all tumors. The study of p53 recognition sites, mdm2, *p21*, and *cyclin G* genes, is important for understanding the role of DNA transcription in cancer. In Figure 5C, the assembly of Au NPs by complementary-strand binding of DNAs, designed using the cyclin *G* promoter sequence, involves Au NPs conjugated with the top and bottom single-stranded DNA (ss-DNA).[14] A double strand is formed by interparticle complementary binding of the two DNAs in between Au NPs, which is a *p53* recognition site. In proof-of-concept demonstration experiments, two different DNA strands, (DNA1:5′-/5ThioMC6-D/AGGCCAGACCTGCCCGGG-CAAGCCTTGGCA-3′ (bottom strand) and DNA2:5′-/5ThioMC6-D/TGCCAAGGCTTGCCCGGG-CAGGTCTGGCCT-3′ (top strand)) were used.[14] For alkanethiolate-capped nanoparticles synthesized in organic phases, the bioconjugation can be achieved by transferring them to aqueous solution via ligand exchange reaction (e.g., mercaptoundecanoic acid) before conjugating with DNAs or proteins.

2.4. Assembly of Nanoparticles with Tunable Optical and Electrical Functions. The interparticle linkage or assembly of NPs leads to changes in optical and spectroscopic properties which provide ways for determining their correlation with the nanoscale parameters (size and composition). Changes in absorbance and wavelength of the surface plasmon (SP) band provide a measure of particle size, shape, concentration and dielectric medium properties, which can be described by Mie theory or SERS intensity. The wavelength (λ_{max}) at maximum absorbance of the SP bands is dependent on the particle size. The increase in the λ_{max} value of the SP band with increased particle size is very comparable between the experimental and the theoretical data. Insights have been developed into the correlation among particle size, SP band, and SERS intensity. For example, the particle size−SERS correlation has been demonstrated by comparison of SERS spectra of Raman labels on Au NPs in solution and on a solid substrate.[20] For Au thin-film substrate immobilized with Au NPs, two intense diagnostic peaks of the MBA were observed at 1081 and 1591 cm^{-1}, displaying a maximum intensity for nanoparticles of 60−70 nm in size (Figure 6A). In contrast, the SERS intensity for MBA adsorbed

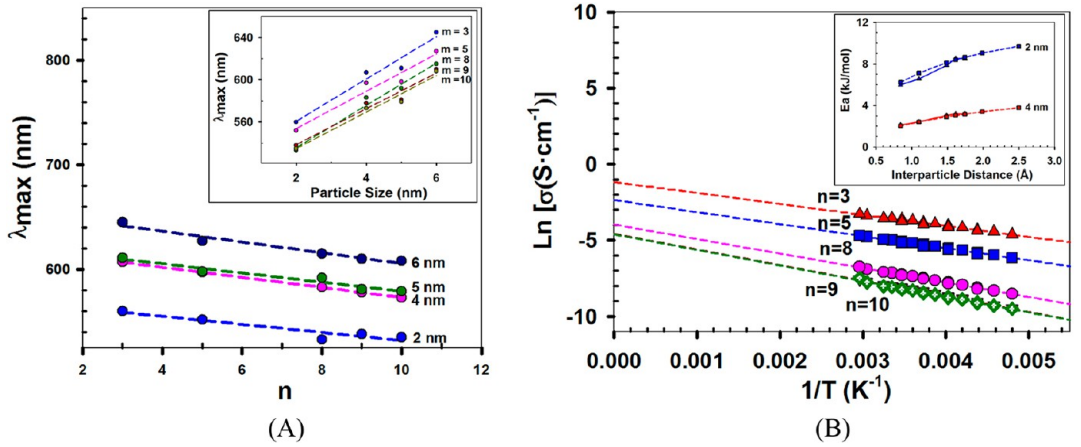

Figure 7. (A) Surface plasmon resonance band wavelength λ_{max} vs. interparticle chain length and particle size (2r, inset) for thin film assemblies of Au NPs mediated by ADTs of different chain lengths (HS-$(CH_2)_n$-SH). (B) Electrical conductivity vs. temperature and interparticle distance for thin film assemblies of 2 nm Au NPs mediated by ADTs of different chain lengths (HS-$(CH_2)_n$-SH). Inset plots, activation energy vs. interparticle distance, and comparison of experimental (solid lines, triangle) and calculated results (dashed lines, square) for two different particle sizes. Reproduced with permission from ref 57, copyright 2007 Royal Society of Chemistry, and from ref 55, copyright 2008 American Chemical Society.

on Au NPs in an aqueous solution shows a gradual increase with the particle size (Figure 6B). The SERS signals are clearly detectable for particle sizes greater than 40 nm. The size correlation of SERS intensity suggests the existence of a critical size range of the nanoparticles in the solution beyond which the particle−particle interaction is operative and responsible for the SERS effect. Because no peak was observed prior to centrifugation, it is likely that the decrease in the interparticle distance between the particles, via formation of small clusters of nanoparticles such as dimers or trimers, allowed more effective plasmonic coupling. The adsorbed MBA molecules confined in such clusters are thus the "hot spots" responsible for the observed SERS effect.

The formation of dimers/trimers is supported by the dependence of the SERS intensity on centrifugation speed and salt concentration. The SERS intensity is found to increase with the speed of centrifugation, which is consistent with the increase in the SP band[12,52] around ∼750 nm characteristic of the nanoparticle aggregation (Figure 6C). Furthermore, while the dimer/trimer formation is also dependent on the salt concentration, the salt-induced aggregation of the MBA-capped nanoparticles is irreversible whereas the centrifugation-induced aggregation of nanoparticles can lead to small clusters, which are dispersible and stable in the solution.

The controlled interparticle linkage could also lead to assembly of the nanoparticles into thin films with changes in optical and electrical properties that are dependent on particle size and interparticle spacing parameters. For example, the SP band for thin film assemblies of Au NPs of different sizes which are linked by alkyl dithiols (ADTs) or carboxylic acid-functionalized thiols (CATs) of different alkyl chain lengths are studied as a model system. It exhibits a red shift of the SP band (λ_{max}) in comparison with the solution counterpart,[55] depending on the chain length (n) (Figure 7A) and the particle diameter (2r) (Figure 7A insert).[55] The correlation of the SP band evolution with particle size, interparticle distance, and dielectric medium properties is in agreement with Mie theory, providing information for assessing the optical properties for the nanostructured thin films.[55] Such optical properties have also been observed for molecularly mediated assembly of AuAg[56] and Fe_3O_4@Au NPs.[43] For example, the SP band for 1,6-hexanedicarboxylic acid (HDA)-mediated assembly of $Au_{23}Ag_{77}$ NPs shifts to longer wavelength (515 nm) in comparison to that before the assembly (460 nm).[56] The SP band shift is a common characteristic for NDT- or MUA-mediated thin film assemblies of Au NPs.

Figure 7B shows the experimentally determined conductivity and activation energy data for ADT-mediated thin film assemblies of Au NPs of two different sizes (2 and 4 nm) and different chain lengths (0.8−2 nm) on interdigitated microelectrodes, revealing a linear dependence on interparticle distance and particle size.[57] On the basis of activated electron tunneling proposed first by Murray et al. in studying the electrical conductivity (σ) of monolayer-protected nanoparticles, the electrical conductivity depends on activation energy (E_A, kJ/mol), T (K), electron coupling term (β), interparticle distance (δ), and intrinsic conductivity of the nanoparticles (σ_0) as defined in Abeles's electrostatic model. The experimental data show very good agreement with the theoretical model in terms of activation energy increase with chain length and decrease with particle size.[58] AuAg nanoparticle thin film assemblies also exhibit similar trends.[56] The detailed electron transport in the nanoparticle films depends on other factors, as evidenced by the observation of CO_2-plasticizing effect on the electrical conductivity.[58]

3. BIOFUNCTIONAL NANOPROBES AND ASSEMBLIES

3.1. Colorimetric Detection of Amino Acids and Small Peptides. Thiol-containing amino acids, such as cysteine (Cys) and homocysteine (Hcys), and small peptides, such as glutathione (GSH), are important biomolecules[6,21,48,52,59,60] because of their linkages to cardiovascular disease and other medical disorders. In the studies of Hcys- and Cys-mediated assembly of Au NPs,[51,52] the interparticle interaction is proposed to involve zwitterion-type electrostatic interaction of the amino acids attached via thiol group on the surface of Au NPs. The change of the SP band as a result of the interparticle interactions enables colorimetric or fluorimetric detection of the amino acids. For glutathione (GSH, a tripeptide and a reducing agent or antioxidant), the assembly of Au NPs involves primarily hydrogen-bonding. In general, the interparticle zwitterion-type electrostatic and hydrogen-bonding interactions of these systems

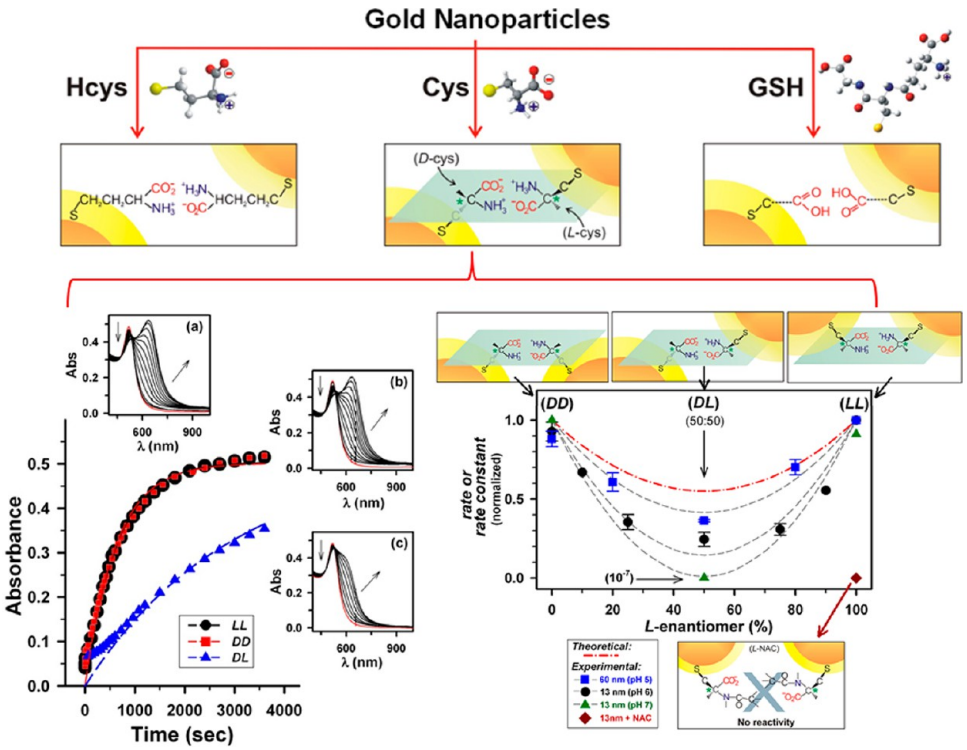

Figure 8. Top: Interparticle zwitterionic interaction, chiral recognition, and hydrogen bonding for the assembly of Au NPs by Hcys, Cys, and GSH. Bottom: (Left) Kinetic plots of SP band absorbance (at 630 nm) for assemblies of $Au_{13\ nm}$ in the presence of LL- (●), DD- (■), and DL- Cys (▲). The dotted lines represent curve fitting by a first-order reaction model. Inset: UV−vis spectral evolution for the $Au_{13\ nm}$ mediated assembly of (a) LL-, (b) DD-, and (c) DL-Cys. The arrows indicate the direction of the spectral evolution. (Right) Normalized rate or rate constant (k) vs enantiomeric percentage of cysteines (%) in the presence of Au NPs of two different sizes: $Au_{60\ nm}$ (pH 5) (■), $Au_{13\ nm}$ (pH 6) (●), and $Au_{13\ nm}$ (pH 7) (▲). Inactivity was also illustrated for mixing $Au_{13\ nm}$ with NAC (♦). Reproduced with permission from ref 60. Copyright 2009 American Chemical Society.

can be illustrated in Figure 8 (top panel). Cys is essential to the function of proteins and enzymes, in which the molecular chirality has important implications to medicine for specific targeting. Chiral recognition of cysteine driven by Au NPs is discovered, as shown in Figure 8 bottom panel.[60]

For the visualization of the nanoparticle-driven pairwise zwitterionic interactions by enantiomeric cysteines adsorbed on Au NPs, imagine a hypothetical quasiplane for the interparticle zwitterion interaction of different chiralities (L and D) (see the structural model), including homochiral (LL and DD) and heterochiral (DL) modes. There are differences between the homochiral and heterochiral interactions based on thermodynamic considerations and computational modeling results. The assembly of Au NPs by interparticle pairwise zwitterionic interaction of the cysteines adsorbed on Au NPs can be monitored by the change of the surface plasmon (SP) resonance band of Au NPs. Upon introducing cysteines into a solution of Au NPs of 13 nm diameter ($Au_{13\ nm}$), and the SP band decreases in absorbance at 520 nm and increases in the ~630 nm region (Figure 8 bottom panel), displaying an isosbestic point at ~540 nm. The apparent rate constant (k) obtained by curve fitting of the SP band evolution using first-order kinetics (Figure 8 bottom panel) shows k values of ~1 order of magnitude greater for the LL and DD assemblies than that for the DL assembly (50% L and 50% D). By modeling the interparticle pairwise dimerization using an idealized model, the heterochiral dimerization is found to be less favorable than the homochiral, which is indeed evidenced by the experimental data ($k_{(DL)} \ll k_{(LL)} \approx k_{(DD)}$), and a minimum reaction rate at an enantiomeric fraction(χ_L) of 50%. The correlation between the apparent rate (r) or k of the interparticle reactivity and the relative concentration of the enantiomer (L%) is shown in Figure 8 bottom panel for Au NPs of two different sizes, revealing a characteristic "valley" feature with the minimum appearing at 50%L:50%D. The important role of the pairwise zwitterionic interaction in the interparticle chiral recognition and nanoparticle assembly is further supported by the inactivity for the assembly of Au NPs using *N*-acetyl-L-cysteine (NAC) as a mediator.

The interparticle homochiral vs. heterochiral reactivities feature preferential interaction and differentiation of the enantiomeric structures, which have important implications to the exploration of the nanoparticle-driven chiral recognition of cysteines in biomedical applications. One example involves early diagnosis and identification of elevated levels of cysteine to medical disorders (e.g., Parkinson's and Alzheimer's). Another potential application is the development of an effective route for controlling the enantiomeric specificity considering the fact that *L*-cysteine's deficiency is associated with a number of clinical situations (liver damage, skin lesions, AIDS, etc.), yet the role in the central nervous system is not well understood and *D*-cysteine interferes with many targets inside the cell. The exploration of the nanoparticle-driven chiral recognition differs from chiralities with single-crystal surfaces and chiral structures on metal NPs mainly in terms of the interparticle chiral reactivity.

3.2. Functional Nanoprobes for Cell Transfection and Bacteria Inactivation. The explorations of functional nanoparticles for cell transfection and bacteria inactivation have attracted increasing interest in recent years because of their potential applications in drug delivery and drug discovery. One

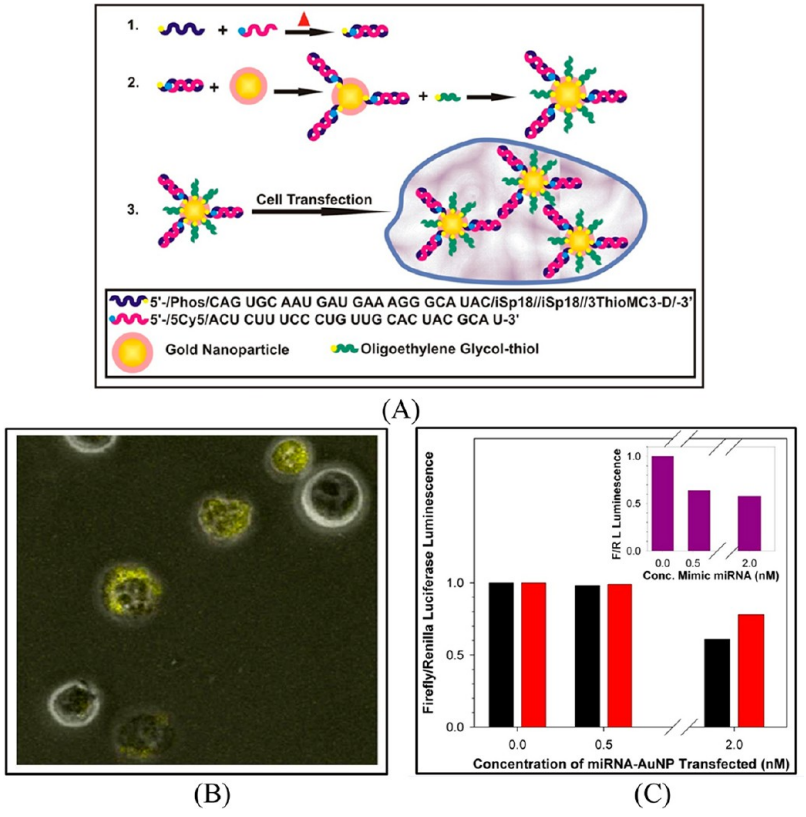

Figure 9. (A) Preparation of miRNA-AuNP conjugates for delivering miRNAs to cells (miRNA is labeled with fluorescent dyes (e.g., Cy5)). The sense and antisense miRNA were combined first to form miRNA duplexes, which are then immobilized onto Au NP via thiol group, followed by refilling with oligoethylene glycol thiol (OEG) to keep the miRNAs from folding and electrostatically binding. (B) Confocal/fluorescent microscopic image: MM.1S cells 48 h after transfection was initiated with Cy5-labeled miRNA-AuNPs. (C) Plot showing the result of the functional luciferase assays for Cy5 (black bars) and Cy3 (red bars) labeled miRNA-AuNPs, and a mimic system (inset chart). Reproduced with permission from ref 51. Copyright 2012 American Chemical Society.

example involves miRNA-conjugated Au NPs for cell transfection, which has potential application in delivering miRNA into cells for genetic manipulation and cancer treatments, such as the resistance of multiple myeloma (MM) to glucocorticoid treatment. The use of Au NPs for the delivery of siRNA (small interfering RNA) into cells for efficient knockdown of target genes without significant cytotoxicity exploits the unique optical properties, low cytotoxicity, and enhanced lifespan in the bloodstream.[61] The manipulation of genetic expression has been demonstrated recently for miR-130b which express differently in glucocorticoid-sensitive versus glucocorticoid-resistant multiple myeloma cell lines (MM.1S). Figure 9A shows a scheme for using miR-130b-conjugated Au NPs in cell transfection. Its overexpression in the MM.1S cell line decreases the expression of a glucocorticoid receptor protein (GR-α), inhibiting glucocorticoid-induced apoptosis of cells.

For demonstrating miRNA-conjugated Au NPs in cell transfection, we used a MM.1S cell line. Figure 9B shows the uptake of the conjugated nanoparticles Cy5-miRNA-AuNPs in the MM.1S cells, as evidenced by the clear contrast in fluorescence from the dye-labeled miRNA-AuNPs. The ability for the conjugated nanoparticles to reduce luciferase expression is further evidenced by functional luciferase assays (Figure 9C). Upon increasing concentration (to 2 nM) of Cy5-miRNA-AuNPs, an observable reduction in gene expression is observed. Considering ~15 miRNAs per Au NP in the miRNA-AuNP solution for the luciferase knockdown and comparing the knockdown efficiencies between siRNA-AuNPs (~20% at 48 h, ~33 siRNAs per particle[50]) and miRNA-AuNPs (~40% at 48 h), the miRNA-AuNPs are found to be more efficient at a much lower concentration[50] for the transfection of the miRNA-AuNPs in multiple myeloma cells.

Another area of interest involves the development of functional antibacterial agents in biological fluids, which stems from the need to store platelets at room temperature where pathogen contamination can occur and pose a risk of infection associated with transfusion. It would be desirable to introduce antibacterial particles in the platelets for inactivating bacteria which can be subsequently separated out prior to transfusion. For Ag NPs, the added value of incorporating magnetic function is the ability of efficient bacterial disinfection with reduced presence of Ag ions in the fluid. One intriguing approach involves the introduction of the magnetic cores into the Ag NPs to enable effective separation, delivery and targeting. This approach is illustrated in Figure 10A for developing magnetic core@Ag NPs for bacterial inactivation in blood platelets. The reduction in bacterial growth of several types of Gram-positive bacteria (e.g., *Staphylococcus aureus* and *Bacillus cereus*) and Gram-negative bacteria (e.g., *Pseudomonas aeruginosa*, *Enterobacter cloacae*, and *Escherichia coli*) has been examined to assess bacterial inactivation efficiency of the functional MZF@Ag NPs. For the growth of Gram-positive *Bacillus cereus* in saline solutions containing antimicrobial NPs over a 24 h period, the bacterial concentration exhibits a clear reduction as a function (Figure 10B (left)). For Gram-negative *Enterobacter cloacae*, an increased speed of inactivation is observed (Figure 10B (middle)).

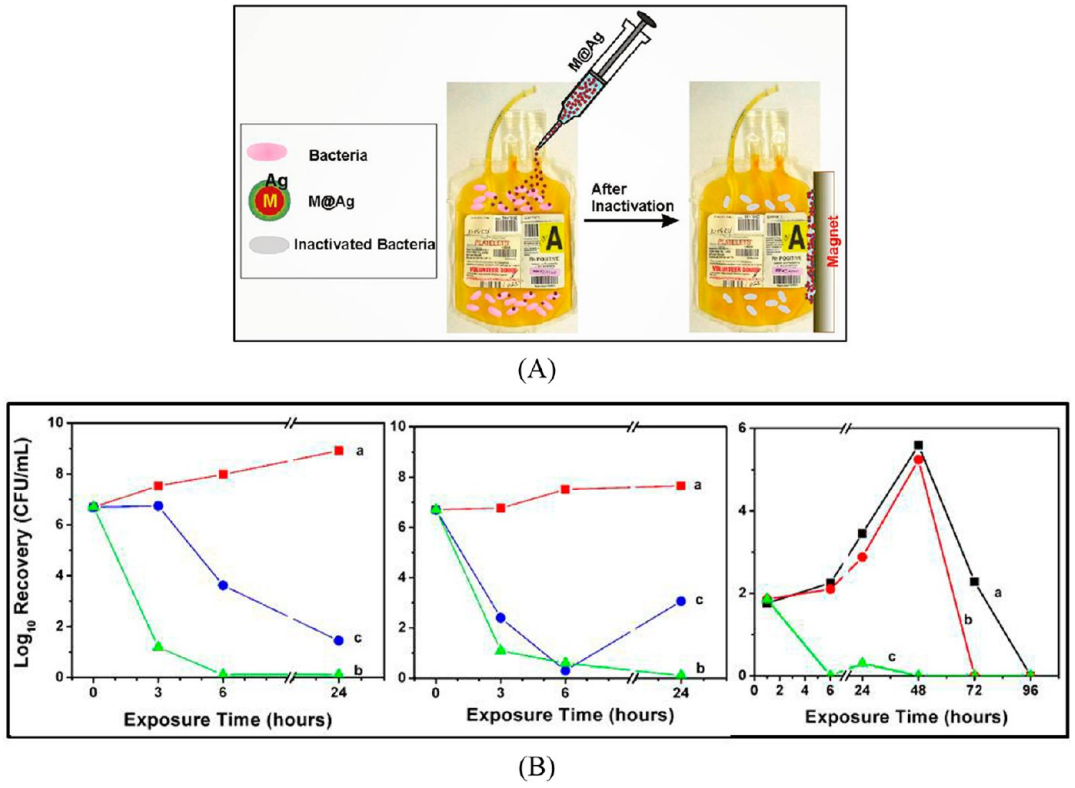

Figure 10. (A) Schematic illustration of magnetic core@shell nanoparticles (M@Ag) as a functional antimicrobial agent in blood platelets and the magnetic separation. (B) Experimental data for the inactivation of *Bacillus cereus* (left) and *Enterobacter cloacae* (middle) in (a) a PBS buffer, (b) a solution of MZF@Ag NPs, and (c) a solution of Ag NPs; and *E. coli* (right) in (a) water, (b) MZF NPs, and (c) MZF@AgNPs in blood platelets. Reproduced with permission from ref 6. Copyright 2011 American Chemical Society.

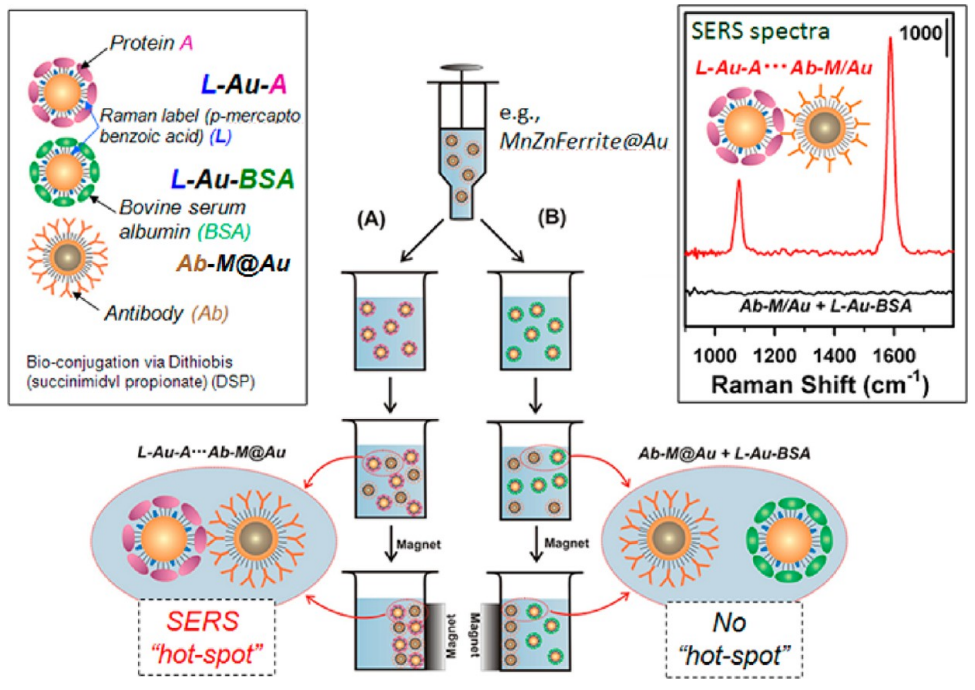

Figure 11. Illustration of functionalized magnetic core (M)@shell (Au) NPs in bioseparation and detection: (A) protein A-labeled Au NPs (L-Au-A) or (B) BSA-labeled Au NPs (L-Au-BSA) and antibody-labeled M@Au nanoparticles (Ab-M@Au). Inset (top-right): SERS spectra showing examples for Au (80 nm) NPs labeled with Protein A or BSA and MBA and M@Au NPs (~8 nm) labeled with antibody (IgG). Reproduced with permission from ref 20. Copyright 2008 IOP Publishing.

For blood platelet samples containing *E. coli*, the inactivation by MZF@AgNPs is also effective, as demonstrated by the drop of bacterial concentration below a detectable level after only 6 h of exposure (Figure 10B (Right)). The inactivation is mainly caused

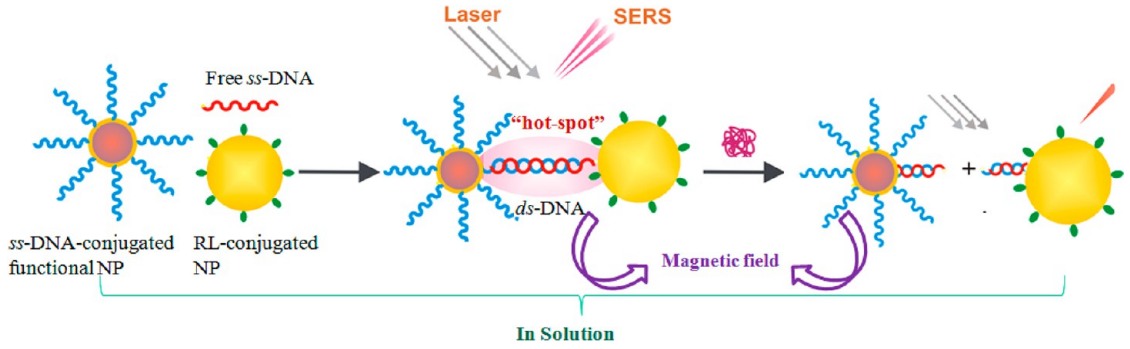

Figure 12. Illustration of formation of "hot-spot" upon *ds*-DNA assembly of *ss*-DNA/M@Au NP with RL-AuNP via molecular recognition with free complementary *ss*-DNA in the solution, and dismantling of "hot-spots" following the enzymatic cutting of the *ds*-DNA using restriction enzyme and magnetic separation characteristic.

by the direct contact of Ag on NPs rather than Ag ions leached into the solution. Considering the low level of the amount of silver found in the platelets, the use of MZF@Ag NPs as a functional antibacterial agent is potentially much safer when giving a transfusion after the removal of the magnetic core−shell nanoparticles. In light of the increasing use of Ag NPs as antimicrobial agent in commercial products in terms of the nanotoxicity,[62] the magnetically functional nanoparticles could offer the ability to reduce the unwanted toxicity, which is clearly desired from the patient or the environment perspectives.

Although the unique properties of metal nanomaterials enable new opportunities in theranostics, some of the nanoparticles may have unpredictable toxic potential upon being released into the environment during use or disposal, either unintentionally (such as during wear and tear), or intentionally (such as nanomedicine). There is a need to evaluate the potential toxic effects of nanoparticles. Although gold-based nanoparticles have shown the least nanotoxicity toward different biological systems in comparison with various nanoparticles, there have been increasing studies to understand the nanotoxicity. For example, exposure to Co and Ni NPs is shown to cause lung inflammation in rats, and oxidative stress and increased matrix metalloproteinase-2 and -9 expression and activity for human monocytes.[63] Several studies also demonstrated that exposure to some metal nanoparticles may cause genotoxic effects. For example, exposure of A549 cells to Co NPs has been shown to cause DNA damage, whereas their exposure to TiO_2 NPs does not cause DNA damage.[64] Exposure to Co NPs is shown to cause an increase in Gadd45α expression in cells which could invoke various cellular responses such as cell cycle arrest, apoptosis, and importantly, DNA repair. Understanding the potential toxic and genotoxic effects of nanoparticles is important for the development of safe nanomaterials for the various applications.

3.3. SERS Detection of Proteins and DNA via Assembly, Disassembly, or Separation. Gold (or silver) nanoparticles and magnetically functional Au or Ag NPs have been demonstrated the viability for SERS detection of the bioreactivity of proteins and DNAs with magnetic separation capability.[20,21] As an important means of sandwich-type immunoassay, SERS readout has the capability of multiplexity.[9] The interparticle assembly between reporter-labeled Au NPs and magnetic core@Au NPs has been exploited for magnetic bioseparation and SERS-based biodetection[20,21] (Figure 11). Attributes such as magnetic separation capability, enhanced stabilization of the magnetic particles, fine-tunable surface to impart biocompatibility have been demonstrated by a number of examples involving the immobilization of recognition sites on Au or M@Au NPs and spectroscopic labels for detection.[20,21] The plasmonic coupling of the localized fields between nanoparticles and substrates produces an enhanced SERS effect,[9,10] as evidenced by the size correlation of the surface plasmon resonance properties for Au NPs.[20] In particular, dimer/trimers of the NPs in the solution via interparticle interactions produce "hot spots"[10] for the SERS effect,[12,22] which is illustrated in Figure 11 insert for developing SERS and magnetic nanoprobes for bioseparation and detection.

As a proof-of-concept demonstration of SERS detection of the protein A-antibody binding activity, Raman label (L = MBA), Protein A (A) and antibody (Ab) are conjugated onto Au and M@Au (or Ag) nanoparticle surfaces.[20,21] Upon applying a magnetic field to the solution containing the reaction product between Protein A capped Au NPs with a Raman label (L-Au-A) and the antibody-capped M@Au NPs (Ab-M@Au), samples are collected and then analyzed. The reactivity with bovine serum albumin (BSA) serves as a control experiment. Diagnostic signals of the MBA are clearly detected for the separated product ((L-Au-A)-(Ab-M@Au) pair) in the SERS spectra. In contrast, there are no signals for the (L-Au-BSA)+(Ab-M@Au) combination in the control experiment using BSA. This proof-of-contrast experiment demonstrates the viability of magnetic nanoprobes for SERS bioassays, which has been supported by a number of examples.[6,20,21,52,59,60]

The creation of the SERS "hot-spot" is an important element of the nanoparticle-based strategy for the detection of DNA bioactivities (Figure 12).[14,17] The use of magnetic nanoparticles with gold or silver shells with a Raman label (RL) has important advantages in overcoming many of the challenging problems in bioprobing. This strategy has in fact attracted both fundamental and practical interests because of potential applications in areas such as ferrofluids, medical imaging, drug targeting and delivery, cancer therapy, separations, and catalysis. A key advantage is the ability of exploiting the rich and controllable surface chemistry and spectroscopic properties of gold or silver while maintaining the magnetic properties of the cores for the desired bioseparation capabilities.

As an expansion to the demonstration of using highly monodispersed gold NPs as SERS-active nanoprobes,[12,21] and M@Au NPs on Au substrates for sandwich-type immunoassay detection,[5,20,21] the small clusters of DNA-linked gold NPs and M@Au or Ag NPs were recently shown to be stable enough in solutions to allow SERS detection of DNAs in terms of assembly and enzymatic cutting.[14,17] The later efforts, built upon our abilities to enable the nanoparticles magnetically functional and/or SERS-active,[6,47] now show promise in terms of proof-of-concept demonstration for the feasibility of the DNA detection,

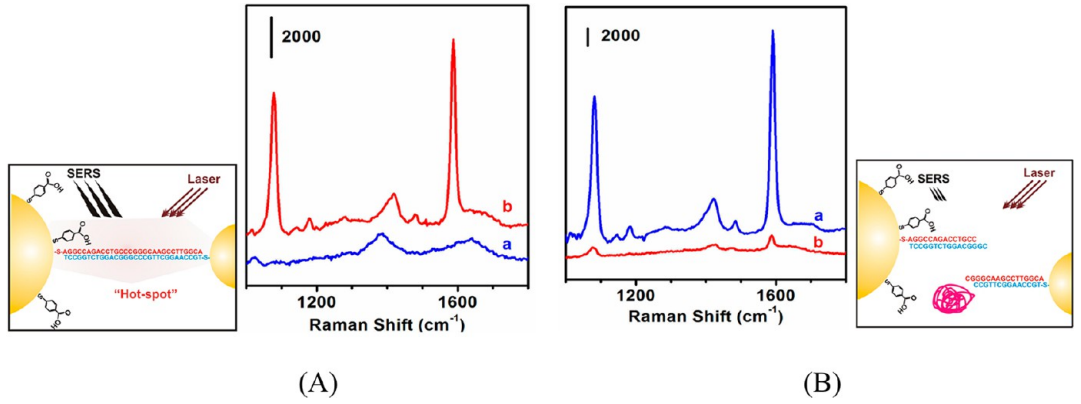

Figure 13. (A) SERS detection of "hot-spot" formation with a 30 bp DNA sequence upon assembly of ss-DNA/AuNP with MBA/AuNP in an aqueous solution ((a) bottom-DNA/AuNP mixed with MBA/AuNP, (b) bottom-DNA/AuNP and MBA/AuNP after addition of top-DNA); and (B) disassembly by cutting the ds-DNA/AuNPs with MspI ((a) the ds-DNA/AuNPs, (b) after MspI addition). Reproduced with permission from ref 14. Copyright 2013 Royal Society of Chemistry.

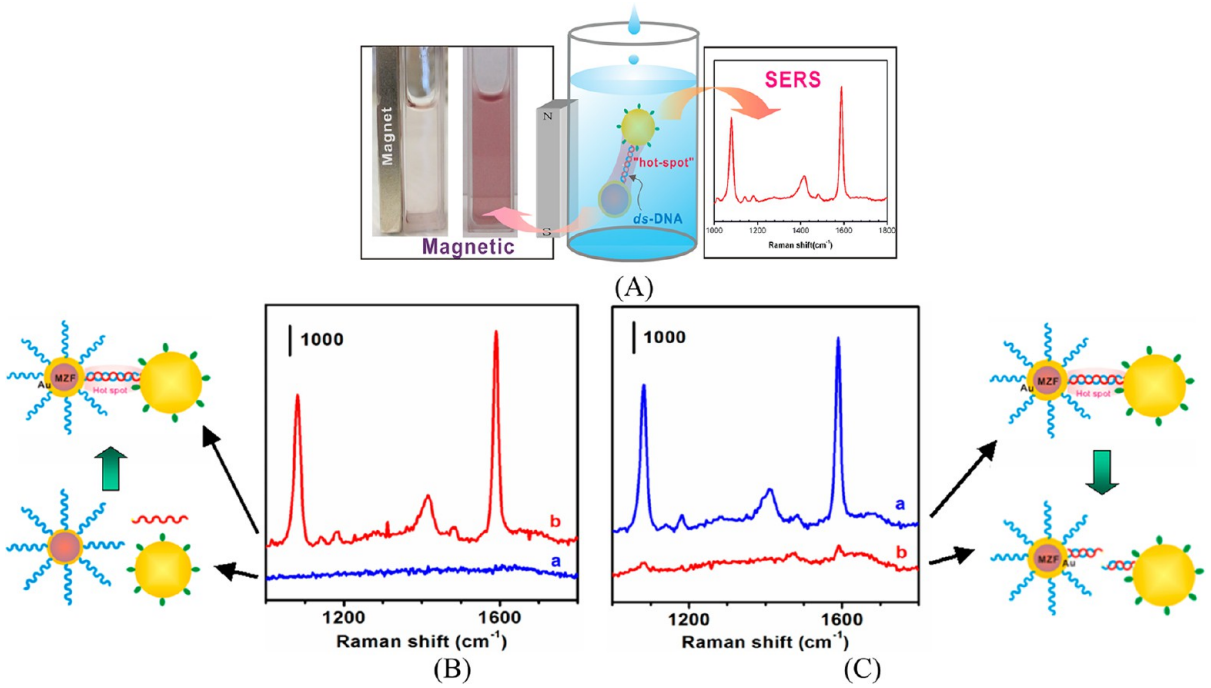

Figure 14. (A) Magnetic NPs coupled with Au NPs for SERS detection. (B) Example using a 30 bp DNA sequence where "hot-spots" form upon the assembly of ss-DNA/MZF@Au with MBA/AuNP in an aqueous solution ((a) the mixture of MBA-Au and MZF/Au-DNA1, and (b) mixture of MZF/Au-DNA1 and MBA-Au in the presence of DNA2). (C) MspI cutting MBA-Au-ds-DNA-MZF/Au ((a) the MBA-Au-ds-DNA-MZF/Au solution; (b) after MspI addition). Reproduced with permission from ref 17. Copyright 2013 Royal Society of Chemistry.

an area related to p53 mutation for cancer diagnostics,[14] and miRNA detection related to cell transfection in cancer therapeutics.[6] Consider first the use of Au NPs of different sizes as nanoprobes for DNA assembly and its enzymatic cutting in an aqueous solution using two different DNA strands with a thiol modification (bottom-DNA and top-DNA, designed using the cyclin G promoter sequence for p53 recognition),[14] the complementary binding of which forms a double strand (ds-DNA). In one solution, Au NPs are conjugated with one of the single-stranded (ss), e.g., ss-bottom-DNA. In another solution, Au NPs are labeled with Raman reporter molecule (e.g., MBA). As shown in Figure 13, by mixing the two solutions in the presence of free top DNA strand, MBA's diagnostic bands can be detected as a result of the formation of ds-DNA-AuNP assemblies with an interparticle "hot-spot".

Figure 13A shows an example where controlled mixing of solutions of 13 nm bottom-DNA/AuNP and 39 nm MBA/AuNP in the presence of top-DNA, a gradual increase of the diagnostic Raman bands of the MBA label is observed at 1078 and 1594 cm^{-1}, corresponding to MBA's ν(CC) ring-breathing modes. Figure 13B shows another example where a restriction enzyme (e.g., MspI) is introduced into the solution of ds-DNA/AuNPs assembly, which is known to cut *ss*-DNAs at CCGG site. A clear decrease in the SERS intensities of the diagnostic peaks at 1078 and 1594 cm^{-1} is revealed, because of the removal of the interparticle "hot-spot" by restriction enzyme cleavage of the ds-DNA, demonstrating the important role of the interparticle "hot-spot" in the SERS detection.

This strategy is expanded to use gold (or silver)-decorated magnetic nanoparticles as nanoprobes for demonstrating DNA

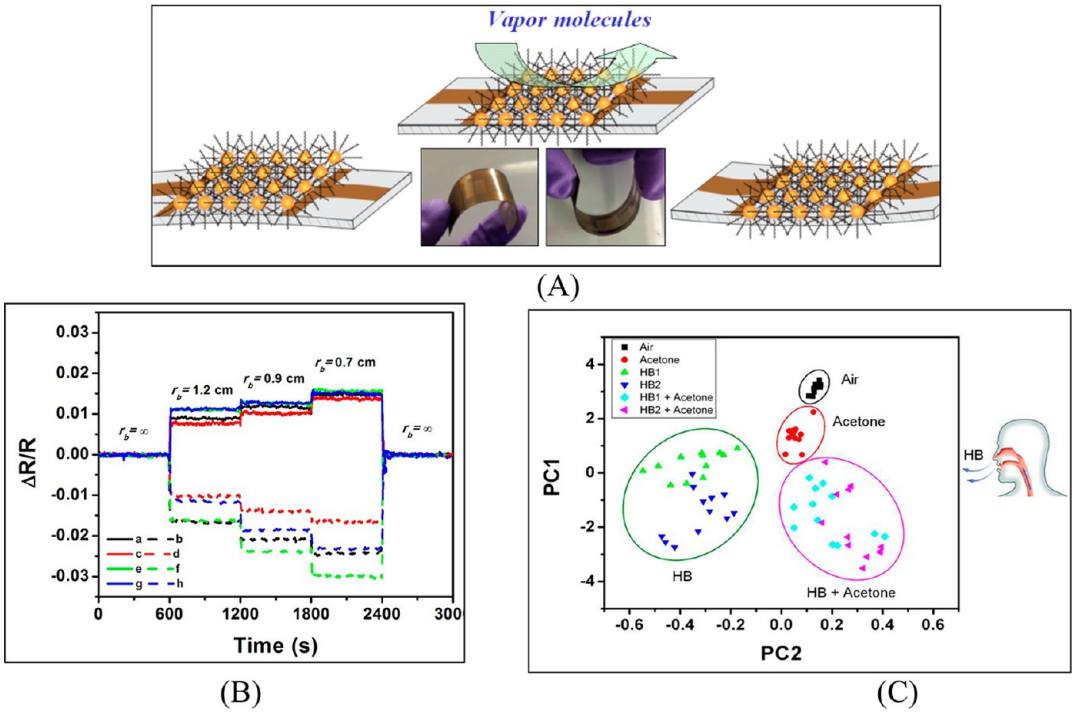

Figure 15. (A) Illustration of thin film of nanoparticles assembled or printed on a flexible chemiresistor device for detection of vapor molecules (VOCs, biomarkers, etc.). (B) Response profiles of relative change in resistance ($\Delta R/R = \Delta R/R_{FL}$) for a flexible device with an NDT−$Au_{2\ nm}$ film in response to horizontal bending under (a, b) nitrogen, (c, d) ethanol, (e, f) hexane, and (g, h) acetone. Strains: solid lines (tensile, ts), dashed lines (compressive, cs). (C) PCA score plots in the PC1-PC2 plane (PC1, 96.8%; PC2, 2.9%.) for a chemiresistor array of thin film assemblies of Au NPs in response to several vapor samples: air (blank), acetone (210 ppm (M) in air), human breath (HB), and HB spiked with acetone. Reproduced with permission from ref 69, Copyright 2014 Royal Society of Chemistry, and from ref 27, Copyright 2012 Elsevier Publishing.

assembly and enzymatic cutting in solutions. Gold- and silver-decorated magnetic MnZn ferrite nanoparticles (MZF@Au or MZF@Ag) have been studied for demonstrating the viability.[17] The distributions of the expected components in MZF@Au, Fe, Mn, Zn, and Au, can be identified in HRTEM and EDS. During the formation of ds-DNA linkage or breakage between Au NPs and MZF@Au (or MZF@Ag) NPs, interparticle "hot-spots" are formed for real-time SERS monitoring of the assembly and enzymatic disassembly processes whereas the magnetic components provide an effective means for intervention in the solution (Figure 14A).

In the case of MZF/Au NPs (11 nm) and MBA-Au NPs (39 nm) forming interparticle ds-DNA of DNA1 and DNA2, two clear SERS peaks are observed at 1078 and 1592 cm^{-1} (Figure 14B), indicative of the interparticle "hot-spot" formation due to assembly of MBA-Au-DNA1/DNA2-MZF/Au, forming dimers or trimers in the solution. Upon addition of MspI into this solution, there is a clear reduction of the two diagnostic peaks (Figure 14C). After the enzymatic cutting, the MZF/Au NPs could be separated from the solution by applying a magnetic field. Similarly, the MZF/Ag NPs were also demonstrated to be viable for SERS detection of the DNA activities and the magnetic intervention after the enzyme cutting process.[17]

In many of the examples such as thiol-containing amino acids, peptides, miRNAs and bacteria, the SERS strategy could also be useful for their detection. For example, polymer-mediated assembly of Au NPs have been used for SERS detection of bacteria biomarker such as dipicolinic acid (DPA) and calcium dipicolinate (Ca-DPA),[65,66] which has application for developing rapid and accurate detection of bacteria in foods or biological fluids. In contrast to Ag NPs traditionally used as SERS substrates for biomarker detection (e.g., *Bacillus subtilis*), the strong SERS effect produced by the particle−particle and particle−substrate plasmonic coupling of Au NPs was demonstrated to exhibit high sensitivity and low detection limit for SERS detection of biomarkers released from bacterial spores.[65,66]

3.4. Chemiresistive Detection of Biomarkers from Human Breath. Molecularly mediated thin film assembly of Au NPs has been demonstrated as sensing materials for chemiresistive detection of breath biomarkers linked to diabetes.[27] The thin films can be prepared by a combination of mediator and template forces in one-step assembly process. This assembly technique builds upon the place-exchange reactivity[37] and expands the layer-by-layer technique.[34] The initial ligand exchange reaction is followed by interparticle linkages. Examples include thiolate-Au bonding on Au NPs, hydrogen-bonding of carboxylic acid terminal groups on Au NPs, and selective carboxylate-Ag bonding on AuAg NPs. For the linker molecules, functionalized molecules are used, including alkyl dithiols (ADT, $HS-(CH_2)_n-SH$), carboxylic acid-functionalized thiols ($HO_2C-(CH_2)_n-SH$), and dicarboxylate acids (DCA, $HO_2C-(CH_2)_n-CO_2H$).[56,57,67] For example, 1,9-nonanedithiol (NDT)-linked thin film assembly of Au NPs involves Au-thiolate bonding at both ends of NDT.[55] These parameters determine the activation energy in a thermally activated conduction path, and thus have an important impact to the electrical signal amplification. The array can be coupled to pattern recognition techniques to enhance selectivity.[67] The design of chemiresistive sensing arrays using the nanoparticle-structured thin films exploits the correlation between the electrical conductivity and the nanostructural parameters such as particle size, interparticle distance, and interparticle dielectric medium properties which determine the

activation energy in a thermally activated conduction path,[68] and the electrical signal amplification. For example, the correlation between the chemiresistive responses to the sorption of volatile organic compounds (VOCs) and the interparticle spatial properties[67] is established for the use of molecularly mediated thin film assemblies of Au and AuAg nanoparticles with ADTs and DCAs of different chain lengths[56] as sensing array elements. Similar to the correlation of interparticle distances with the collective electrical or optical properties,[55,57,67] the balance of the interparticle chain−chain cohesive interdigitation and the nanostructure−vapor interaction is an important factor for the correlation between the sensor array's sensitivity or selectivity and the interparticle spatial properties. The interparticle spatial properties play a dominant role in the sensor response characteristics.

This work is recently expanded to flexible chemical/bio sensors for scalable thin-film assembly and printing on flexible substrates that allow exploring the unique electrical/optical properties under various device strains for detection of chemical, biological or biomarker molecules (Figure 15A).[68,69] One important aspect of the flexible chemical and gauge sensors explores the unique correlation between chemical sensing and device strain characteristics under different vapor/gas atmospheres. A major finding is that an increase in resistance is observed in tensile strain (ts), and a decrease in the compressive strain (cs), displaying ΔR in the order of (hexane) > (nitrogen) ≈ (acetone) > (ethanol) (Figure 15B). The increase of the interparticle distance is responsible for the increase of resistance in the case of tensile strain, whereas the decrease of the interparticle distance leads to a decrease of resistance in the case of compressive strain. The overall changes reflect a combination of the interparticle spatial and dielectric properties as a result of vapor sorption in the thin film, which follow the theoretical prediction for some cases. This study demonstrated the ability to tune the interparticle interactions via capping or linking molecules that can work cooperatively with the device strains and chemical environment over the device, an important feature for multifunctional devices.

To explore the sensor arrays with assembled or printed nanoparticle thin films for chemical sensing of biomarkers in human breath linked to diabetes or lung cancers, a preliminary proof-of-concept experiment (Figure 15C) has demonstrated the viability. In addition to showing the viability for quantitative detection of acetone, the results from the array's response data to different samples of human breaths (HB1 and HB2) along with the various control experiments have demonstrated that the sensor arrays with nanostructured sensing films are viable for the detection of acetone, which is a volatile biomarker in diabetics' breath. The initial results have demonstrated the potential of the sensor arrays coupled with pattern recognition for the detection of acetone. Further optimization of the performance parameters could lead to portable and noninvasive monitoring of diabetes.[68,69,27] As shown by the PC1-PC2 plots in Figure 15C, air, acetone, human breath, and acetone-spiked human breath samples are clearly separated, demonstrating the feasibility of distinguishing human breath (with or without spiked acetone) from air (with or without acetone), as well as the potential of the sensor arrays coupled with pattern recognition for the detection of acetone in diabetic breath.

In these illustrated examples, the ligand-framework nanostructures are exploited in terms of electrical and mass transfer properties. For many other nanoparticle assemblies that are structurally defined for harnessing the collective nanoscale electrical, optical, magnetic and spectroscopic properties, the basic principles are expected to operate similarly. A wide range of technological applications should benefit from further detailed delineation of the interparticle parameters in terms of size, shape, composition, and surface properties to optimize the multifunctional optical, magnetic, and spectroscopic properties of the molecularly mediated thin film assembly of nanoparticles.

4. SUMMARY AND FUTURE PERSPECTIVES

In summary, significant progress has been made toward harnessing the metal nanoparticles and assemblies as an effective strategy to create multifunctional properties for detection, targeting, recognition, and diagnostics. Many of the examples of the multifunctional properties discussed in this article have focused on the optical, spectroscopic, electrical and magnetic properties for signal transduction or process intervention in a wide range of molecular or biomolecular systems such as amino acids, peptides, proteins, DNAs, miRNAs, bacteria, and biomarkers. These multifunctional properties are often linked to the interparticle interactions and reactivities at the interfaces between the nanoparticles and the targeted biomolecules. The examples illustrate the importance of understanding the detailed nanostructural parameters such as size, composition and surface properties in correlation with their optical, spectroscopic, electrical, and magnetic properties, and with their potential nanotoxicity. There are also other nanostructural parameters such as shape and interatomic distance or geometry and other material properties such as catalytic and thermoelectric properties, which can regulate the interfacial interactions and reactivities for the nanotransduction and nanointervention, which are not discussed in this article but are actively investigated by many researchers, including us in previous and ongoing efforts.

To expand the scope of the nanotransduction and nanointervention to various theranostic applications, two of the research fronts are becoming increasingly active. One involves a fundamental understanding of the design parameters in nanoengineering of the functional nanoparticles in terms of the desired (e.g., specific targeting) and undesired (e.g., nanotoxicity effect) properties. This front is in fact showing rapid progress with the help of many high energy or high-resolution analytical capabilities to probe the detailed atomic-scale structures using composition mapping and synchrotron X-ray based techniques. The other front involves scalable and low-cost fabrication of the functional nanoparticles and assemblies on scalable platforms to enable their practical applications as theranostic materials in detection and imaging. The latter would allow establishing practically viable devices or technologies for diseases and cancer biomarker detection. The importance of this front is reflected by many emerging research activities focusing on point-of-care detection devices and low-cost printable and flexible sensing devices. The progress in these fronts will provide both fundamental and practical knowledge for advancing nanoparticle-based theranostic materials.

■ AUTHOR INFORMATION

Corresponding Author

*E-mail: cjzhong@binghamton.edu. Phone: (607) 777-4605.

Author Contributions

†Z.S. and H.C. contributed equally to writing this manuscript as cofirst authors.

Notes

The authors declare no competing financial interest.

■ ACKNOWLEDGMENTS

The authors express their appreciations to former and current members of the Zhong Research Group and collaborators who have made contributions to the work described in this article. Portions of the research are supported by the National Science Foundation (CMMI 1100736) and SUNY Research Collaboration Fund.

■ REFERENCES

(1) Agasti, S. S.; Rana, S.; Park, M. H.; Kim, C. K.; You, C. C.; Rotello, V. M. Nanoparticles for Detection and Diagnosis. *Adv. Drug Delivery Rev.* **2010**, *62*, 316−328.

(2) Zhang, X. Q.; Xu, X. Y.; Lam, R.; Giljohann, D.; Ho, D.; Mirkin, C. A. Strategy for Increasing Drug Solubility and Efficacy through Covalent Attachment to Polyvalent DNA-Nanoparticle Conjugates. *ACS Nano* **2011**, *5*, 6962−9670.

(3) Hnilova, M.; Khatayevich, D.; Carlson, A.; Oren, E. E.; Gresswell, C.; Zheng, S.; Ohuchi, F.; Sarikaya, M.; Tamerler, C. Single-Step Fabrication of Patterned Gold Film Array by an Engineered Multi-Functional Peptide. *J. Colloid Interface Sci.* **2012**, *365*, 97−102.

(4) Koch, M.; Kiefer, S.; Cavelius, C.; Kraegeloh, A. Use of a Silver Ion Selective Electrode to Assess Mechanisms Responsible for Biological Effects of Silver Nanoparticles. *J. Nanopart. Res.* **2012**, *14*, 646−657.

(5) Lim, I-I. S.; Zhong, C. J. Molecularly-Mediated Processing and Assembly of Nanoparticles: Exploring the Interparticle Interactions and Structures. *Acc. Chem. Res.* **2009**, *42*, 798−808.

(6) Wang, L. Y.; Luo, J.; Shan, S. Y.; Crew, E.; Yin, J.; Wallek, B.; Wong, S.; Zhong, C.J. Bacterial Inactivation using Silver-coated Magnetic Nanoparticles as Functional Antimicrobial Agents. *Anal. Chem.* **2011**, *83*, 8688−8695.

(7) Wang, Y. Q.; Yan, B.; Chen, L. X. SERS Tags: Novel Optical Nanoprobes for Bioanalysis. *Chem. Rev.* **2013**, *113*, 1391−1428.

(8) Kneipp, J.; Kneipp, H.; Rice, W. L.; Kneipp, K. Optical Probes for Biological Applications Based on Surface-Enhanced Raman Scattering from Indocyanine Green on Gold Nanoparticles. *Anal. Chem.* **2005**, *77*, 2381−2385.

(9) Driskell, J. D.; Lipert, R. J.; Porter, M. D. Labeled Gold Nanoparticles Immobilized at Smooth Metallic Substrates: Systematic Investigation of Surface Plasmon Resonance and Surface-Enhanced Raman Scattering. *J. Phys. Chem. B* **2006**, *110*, 17444−17451.

(10) Hao, E.; Schatz, G. C. Electromagnetic Fields Around Silver Nanoparticles and Dimers. *J. Chem. Phys.* **2004**, *120*, 357−366.

(11) Barhoumi, A.; Zhang, D.; Tam, F.; Halas, N. J. Surface-Enhanced Raman Spectroscopy of DNA. *J. Am. Chem. Soc.* **2008**, *130*, 5523−5529.

(12) Njoki, P. N.; Luo, J.; Kamundi, M. M.; Lim, I-I. S.; Zhong, C. J. Aggregative Growth in Size-Controlled Growth of Monodispersed Gold Nanoparticles. *Langmuir* **2010**, *26*, 13622−13629.

(13) Stoeva, S. I.; Huo, F.; Lee, J. S.; Mirkin, C. A. Three-Layer Composite Magnetic Nanoparticle Probes for DNA. *J. Am. Chem. Soc.* **2005**, *127*, 15362−15363.

(14) Crew, E.; Yan, H.; Lin, L. Q.; Skeete, Z.; Kotlyar, T.; Tchah, N.; Lee, J.; Bellavia, M.; Goodshaw, I.; Joseph, P.; Luo, J.; Gal, S.; Zhong, C. J. DNA Assembly and Enzymatic Cutting in Solutions: a Gold Nanoparticle Based SERS Detection Strategy. *Analyst* **2013**, *138*, 4941−4949.

(15) Bonham, A. J.; Braun, G.; Pavel, I.; Moskovits, M.; Reich, N. O. Detection of Sequence-Specific Protein-DNA Interactions via Surface Enhanced Resonance Raman Scattering. *J. Am. Chem. Soc.* **2007**, *129*, 14572−14573.

(16) Sun, L.; Yu, C.; Irudayaraj, J. Surface-Enhanced Raman Scattering Based Nonfluorescent Probe for Multiplex DNA Detection. *Anal. Chem.* **2007**, *79*, 3981−3988.

(17) Lin, L. Q.; Crew, E.; Yan, H.; Shan, S.; Skeete, Z.; Mott, D.; Krentsel, T.; Yin, J.; Chernova, N. A.; Luo, J.; Engelhard, M. H.; Wang, C.; Li, Q. B.; Zhong, C. J. Bifunctional Nanoparticles for SERS Monitoring and Magnetic Intervention of Assembly and Enzyme Cutting of DNAs. *J. Mater. Chem. B* **2013**, *1*, 4320−4330.

(18) Lim, D. K.; Jeon, K. S.; Hwang, J. H.; Kim, H.; Kwon, S.; Suh, Y. D.; Nam, J. M. Highly Uniform and Reproducible Surface-Enhanced Raman Scattering from DNA-tailorable Nanoparticles with 1-nm Interior Gap. *Nat. Nanotechnol.* **2011**, *6*, 452−460.

(19) Doering, W. E.; Piotti, M. E.; Natan, M. J.; Freeman, R. G. SERS as a Foundation for Nanoscale, Optically Detected Biological Labels. *Adv. Mater.* **2007**, *19*, 3100−3108.

(20) Lim, I-I. S.; Njoki, P. N.; Park, H. Y.; Wang, X.; Wang, L.; Mott, D.; Zhong, C. J. Gold and Magnetic Oxide/Gold Core/Shell Nanoparticles as Bio-Functional Nanoprobes. *Nanotechnology* **2008**, *19*, 305102.

(21) Park, H. Y.; Schadt, M. J.; Wang, L.; Lim, I-I. S.; Njoki, P. N.; Kim, S. H.; Jang, M. Y.; Luo, J.; Zhong, C. J. Fabrication of Magnetic Core@Shell Fe-Oxide@Au Nanoparticles for Interfacial Bio-activity and Bio-separation. *Langmuir* **2007**, *23*, 9050−9056.

(22) Yan, H.; Lim, I-I. S.; Zhang, L. C.; Gao, S. C.; Mott, D.; Le, Y.; An, D. L.; Zhong, C. J. Rigid, Conjugated and Shaped Arylethynes as Mediators for the Assembly of Gold Nanoparticles. *J. Mater. Chem.* **2011**, *21*, 1890−1901.

(23) Alvarez-Puebla, R. A.; Liz-Marzán, L. M. Traps and Cages for Universal SERS Detection. *Chem. Soc. Rev.* **2012**, *41*, 43−51.

(24) Hultman, K. L.; Raffo, A. J.; Grzenda, A. L.; Harris, P. E.; Brown, T. R.; O'Brien, S. Magnetic Resonance Imaging of Major Histocompatibility Class II Expression in the Renal Medulla Using Immunotargeted Superparamagnetic Iron Oxide Nanoparticles. *ACS Nano* **2008**, *2*, 477−484.

(25) Jun, B. H.; Noh, M. S.; Kim, J. Y.; Kim, G. S.; Kang, H. M.; Kim, M. S.; Seo, Y. T.; Baek, J. H.; Kim, J. H.; Park, J. Y.; Kim, S. Y.; Kim, Y. K.; Hyeon, T. W.; Cho, M. H.; Jeong, D. H.; Lee, Y. S. Multifunctional Silver-Embedded Magnetic Nanoparticles as SERS Nanoprobes and Their Applications. *small* **2010**, *6*, 119−125.

(26) Qian, X. M.; Zhou, X.; Nie, S. M. Surface-Enhanced Raman Nanoparticle Beacons Based on Bioconjugated Gold Nanocrystals and Long Range Plasmonic Coupling. *J. Am. Chem. Soc.* **2008**, *130*, 14934−14935.

(27) Luo, J.; Luo, J.; Wang, L.; Shi, X.; Yin, J.; Crew, E.; Lu, S.; Lesperance, L. M.; Zhong, C. J. Nanoparticle-Structured Thin Film Sensor Arrays for Breath Sensing. *Sens. Actuators, B* **2012**, *161*, 845−854.

(28) Peng, G.; Tisch, U.; Adams, O.; Hakim, M.; Shehada, N.; Broza, Y. Y.; Billan, S.; Abdah-Bortnyak, R.; Kuten, A.; Haick, H. Diagnosing Lung Cancer in Exhaled Breath Using Gold Nanoparticles. *Nat. Nanotechnol.* **2009**, *4*, 669−673.

(29) Buszewski, B.; Grzywinski, D.; Ligor, T.; Stacewicz, T.; Bielecki, Z.; Wojtas, J. Detection of Volatile Organic Compounds as Biomarkers in Breath Analysis by Different Analytical Techniques. *Bioanalysis* **2013**, *5*, 2287−2306.

(30) Ye, S.; Mao, Y.; Guo, Y.; Zhang, S. Enzyme-based Signal Amplification of Surface-Enhanced Raman Scattering in Cancer-biomarker Detection. *TrAC* **2014**, *55*, 43−54.

(31) Barrow, S. J.; Funston, A. M.; Wei, X.; Mulvaney, P. DNA-Directed Self-assembly and Optical Properties of Discrete 1D, 2D and 3D Plasmonic Structures. *Nano Today* **2013**, *8*, 138−167.

(32) Wang, L.; Xu, L.; Kuang, H.; Xu, C.; Kotov, N. A. Dynamic Nanoparticle Assemblies. *Acc. Chem. Res.* **2012**, *45*, 1916−1926.

(33) Jones, M. R.; Osberg, K. D.; Macfarlane, R. J.; Langille, M. R.; Mirkin, C. A. Templated Techniques for the Synthesis and Assembly of Plasmonic Nanostructures. *Chem. Rev.* **2011**, *111*, 3736−3827.

(34) Shields, S. P.; Richards, V. N.; Buhro, W. E. Nucleation Control of Size and Dispersity in Aggregative Nanoparticle Growth. a Study of the Coarsening Kinetics of Thiolate-Capped Gold Nanocrystals. *Chem. Mater.* **2010**, *22*, 3212−3225.

(35) Saha, K.; Agasti, S. S.; Kim, C.; Li, X. N.; Rotello, V. M. Gold Nanoparticles in Chemical and Biological Sensing. *Chem. Rev.* **2012**, *112*, 2739−2779.

(36) Brust, M.; Walker, M.; Bethell, D.; Schiffrin, D. J.; Whyman, R. Synthesis of Thiol-Derivatized Gold Nanoparticles in a 2-Phase Liquid-Liquid System. *Chem. Commun.* **1994**, *7*, 801−802.

(37) Schadt, M. J.; Cheung, W.; Luo, J.; Zhong, C. J. Molecularly-Tuned Size Selectivity in Thermal Processing of Gold Nanoparticles. *Chem. Mater.* **2006**, *18*, 5147−5149.
(38) Maye, M. M.; Zheng, W. X.; Leibowitz, F. L.; Ly, N. K.; Zhong, C. J. Heating-Induced Evolution of Thiolate-Encapsulated Gold Nanoparticles: a Strategy for Size and Shape Manipulations. *Langmuir* **2000**, *16*, 490−497.
(39) Hostetler, M. J.; Wingate, J. E.; Zhong, C. J.; Harris, Y. E.; Vachet, R. W.; Clark, M. R.; Londono, J. D.; Green, S. J.; Stokes, J. J.; Wignall, G. D.; Glish, G. L.; Porter, M. D.; Evans, N. D.; Murray, R. W. Alkanethiolate Gold Cluster Monolayers with Radii from 7 to 26 Angstroms: Borders between Molecular and Metallic Behavior and between Two- and Three-dimensional Monolayers. *Langmuir* **1998**, *14*, 17−30.
(40) Wang, F.; Richards, V. N.; Shields, S. P.; Buhro, W. E. Kinetics and Mechanisms of Aggregative Nanocrystal Growth. *Chem. Mater.* **2014**, *26*, 5−21.
(41) Kariuki, N. N.; Luo, J.; Maye, M. M.; Hassan, A.; Menard, T.; Naslund, H. R.; Lin, Y.; Wang, C.; Engelhard, M. H.; Zhong, C. J. Composition-Controlled Synthesis of Bimetallic Gold-Silver Nanoparticles. *Langmuir* **2004**, *20*, 11240−11246.
(42) Lahtinen, R. M.; Mertens, S. F. L.; East, E.; Kiely, C. J.; Schiffrin, D. J. Silver Halide Colloid Precursors for the Synthesis of Monolayer-Protected Clusters. *Langmuir* **2004**, *20*, 3289−3296.
(43) Wang, L. Y.; Luo, J.; Fan, Q.; Suzuki, M.; Suzuki, I. S.; Engelhard, M. H.; Lin, Y.; Kim, N.; Wang, J. Q.; Zhong, C. J. Synthesis and Characterization of Monolayer-Capped PtVFe Nanoparticles with Controllable Sizes and Composition. *J. Phys. Chem. B* **2005**, *109*, 21593−21601.
(44) Wang, X.; Wang, L.; Lim, I-I. S.; Bao, K.; Mott, D.; Park, H. Y.; Luo, J.; Hao, S.; Zhong, C. J. Synthesis, Characterization and Potential Application of MnZn Ferrite and MnZn Ferrite@Au Nanoparticles. *J. Nanosci. Nanotechnol.* **2009**, *9*, 3005−3012.
(45) Sun, S. H.; Zeng, H.; Robinson, D. B.; Raoux, S.; Rice, P. M.; Wang, S. X.; Li, G. X. Monodisperse MFe_2O_4 (M = Fe, Co, Mn) Nanoparticles. *J. Am. Chem. Soc.* **2004**, *126*, 273−279.
(46) Luo, J.; Wang, L. Y.; Mott, D.; Njoki, N. P.; Lin, Y.; He, T.; Xu, Z.; Wanjana, B.; Lim, I-I. S.; Zhong, C.J. Core@Shell Nanoparticles as Electrocatalysts for Fuel Cell Reactions. *Adv. Mater.* **2008**, *20*, 4342−4347.
(47) Wang, L.; Wang, X.; Luo, J.; Wanjala, B. N.; Wang, C.; Chernova, N.; Engelhard, M. H.; Bae, I. T.; Liu, Y.; Zhong, C. J. Core-Shell Structured Ternary Magnetic Nanocubes. *J. Am. Chem. Soc.* **2010**, *132*, 17686.
(48) Zeng, H.; Rice, P. M.; Wang, S. X.; Sun, S. Shape-Controlled Synthesis and Shape-Induced Texture of $MnFe_2O_4$ Nanoparticles. *J. Am. Chem. Soc.* **2004**, *126*, 11458−11459.
(49) Nagaraja, A. K.; Creighton, C. J.; Yu, Z. F.; Zhu, H. F.; Gunaratne, P. H.; Reid, J. G.; Olokpa, E.; Itamochi, H.; Ueno, N. T.; Hawkins, S. M.; Anderson, M. L.; Matzuk, M. M. A Link between mir-100 and FRAP1/mTOR in Clear Cell Ovarian Cancer. *Mol. Endocrinol.* **2010**, *24*, 447−463.
(50) Giljohann, D. A.; Seferos, D. S.; Prigodich, A. E.; Patel, P. C.; Mirkin, C. A. Gene Regulation with Polyvalent siRNA-Nanoparticle Conjugates. *J. Am. Chem. Soc.* **2009**, *131*, 2072−2073.
(51) Crew, E.; Tessel, M. A.; Rahman, S.; Razzak-Jaffar, A.; Mott, D.; Kamundi, M.; Yu, G.; Tchah, N.; Lee, J.; Bellavia, M.; Zhong, C. J. MicroRNA Conjugated Gold Nanoparticles and Cell Transfection. *Anal. Chem.* **2012**, *84*, 26−29.
(52) Lim, I-I. S.; Ip, W.; Crew, E.; Njoki, P. N.; Mott, D.; Zhong, C. J.; Pan, Y.; Zhou, S. Homocysteine-Mediated Reactivity and Assembly of Gold Nanoparticles. *Langmuir* **2007**, *23*, 826−833.
(53) Jin, R.; Wu, G.; Li, Z.; Mirkin, C. A.; Schatz, G. C. What Controls the Melting Properties of DNA-Linked Gold Nanoparticles Assemblies? *J. Am. Chem. Soc.* **2003**, *125*, 1643−1654.
(54) Lytton-Jean, A. K. R.; Han, M. S.; Mirkin, C. A. Microarray Detection of Duplex and Triplex DNA Binders with DNA-Modified Gold Nanoparticles. *Anal. Chem.* **2007**, *79*, 6037−6041.
(55) Wang, L. Y.; Miller, D.; Fan, Q.; Luo, J.; Schadt, M.; Rendeng, Q.; Wang, G. R.; Wang, J.; Kowach, G. R.; Zhong, C. J. Assessment of Morphological and Optical Properties of Molecularly-Mediated Thin Film Assembly of Gold Nanoparticles. *J. Phys. Chem. C* **2008**, *112*, 2448−2455.
(56) Kariuki, N. N.; Luo, J.; Hassan, A.; Lim, I-I. S.; Wang, L. Y.; Zhong, C. J. Assembly of Bimetallic Gold-Silver Nanoparticles via Selective Interparticle Dicarboxylate-Silver Linkages. *Chem. Mater.* **2006**, *18*, 123−132.
(57) Wang, G. R.; Wang, L. Y.; Rendeng, Q.; Wang, J.; Luo, J.; Zhong, C. J. Correlation between Nanostructural Parameters and Conductivity Properties for Thin Film Assemblies of Gold Nanoparticles. *J. Mater. Chem.* **2007**, *17*, 457−462.
(58) Choi, J. P.; Coble, M. M.; Branham, M. R.; DeSimone, J. M.; Murray, R. W. Dynamics of CO^{2}-Plasticized Electron Transport in Au Nanoparticle Films: Opposing Effects of Tunneling Distance and Local Site Mobility. *J. Phys. Chem. C* **2007**, *111*, 3778−3785.
(59) Lim, I-I. S.; Mott, D.; Ip, W.; Njoki, P. N.; Pan, Y.; Zhou, S.; Zhong, C. J. Interparticle Interactions in Glutathione Mediated Assembly of Gold Nanoparticles. *Langmuir* **2008**, *24*, 8857−8863.
(60) Lim, I-I. S.; Mott, D.; Engelhard, M.; Pan, Y.; Kamodia, S.; Luo, J.; Njoki, P. N.; Zhou, S.; Wang, L.; Zhong, C. J. Interparticle Chiral Recognition of Enantiomers: a Nanoparticle-Based Regulation Strategy. *Anal. Chem.* **2009**, *81*, 689−698.
(61) Prencipe, G.; Tabakman, S. M.; Welsher, K.; Liu, Z.; Goodwin, A. P.; Zhang, L.; Henry, J.; Dai, H. J. PEG Branched Polymer for Functionalization of Nanomaterials with Ultralong Blood Circulation. *J. Am. Chem. Soc.* **2009**, *131*, 4783−4787.
(62) Johnston, H. J.; Hutchison, G.; Christensen, F. M.; Peters, S.; Hankin, S.; Stone, V. A Review of the in Vivo and in Vitro Toxicity of Silver and Gold Particulates: Particle Attributes and Biological Mechanisms Responsible for the Observed Toxicity. *Crit. Rev. Toxicol.* **2010**, *40*, 328−346.
(63) Wan, R.; Mo, Y.; Chien, S.; Li, Y.; Li, Y.; Tollerud, D. J.; Zhang, Q. The Role of Hypoxia Inducible Factor-1 Alpha in the Increased MMP-2 and MMP-9 Production by Human Monocytes Exposed to Nickel Nanoparticles. *Nanotoxicology* **2011**, *5*, 568−582.
(64) Wan, R.; Mo, Y.; Feng, L.; Chien, S.; Tollerud, D. J.; Zhang, Q. DNA Damage Caused by Metal Nanoparticles: Involvement of Oxidative Stress and Activation of ATM. *Chem. Res. Toxicol.* **2012**, *25*, 1402−1411.
(65) Cheng, H. W.; Huan, S. Y.; Yu, R. Q. Nanoparticle-Based Substrates for Surface-Enhanced Raman Scattering Detection of Biomolecules. *Analyst* **2012**, *137*, 3601−3608.
(66) Cheng, H. W.; Huan, S. Y.; Wu, H. L.; Shen, G. L.; Yu, R. Q. Surface-Enhanced Raman Spectroscopic Detection of Biomarker Using Gold Nanoparticle Immobilized Substrates. *Anal. Chem.* **2009**, *81*, 9902−9912.
(67) Wang, L. Y.; Shi, X.; Kariuki, N. N.; Schadt, M. J.; Wang, G. R.; Rendeng, Q.; Choi, J.; Luo, J.; Lu, S.; Zhong, C. J. Array of Molecularly-Mediated Thin Film Assemblies of Nanoparticles: Correlation of Vapor Sensing with Interparticle Spatial Properties. *J. Am. Chem. Soc.* **2007**, *129*, 2161−2170.
(68) Yin, J.; Hu, P.; Luo, J.; Wang, L.; Cohen, M. F.; Zhong, C. J. Molecularly−Mediated Thin Film Assembly of Nanoparticles on Flexible Devices: Electrical Conductivity vs. Device Strains in Different Gas/Vapor Environment. *ACS Nano* **2011**, *5*, 6516−6526.
(69) Shan, S.; Zhao, W.; Luo, J.; Yin, J.; Switzer, J. C.; Joseph, P.; Lu, S.; Poliks, M.; Zhong, C. J. Flexibility Characteristics of a Polyethylene Terephthalate Chemiresistor Coated with a Nanoparticle Thin Film Assembly. *J. Mater. Chem. C* **2014**, *2*, 1893−1903.